Microstructure and deformation micromechanisms of concentrated fiber bundle suspensions: An analysis combining x-ray microtomography and pull-out tests

O. Guiraud and L. Orgéas[a]

Laboratoire Sols-Solides-Structures-Risques (3SR Lab), CNRS/Université de Grenoble (Grenoble INP/UJF), BP 53, 38041 Grenoble Cedex 9, France

P. J. J. Dumont

Laboratoire de Génie des Procédés Papetiers (LGP2), CNRS/Université de Grenoble (Grenoble INP), 461 rue de la Papeterie, BP 65, 38402 Saint-Martin-d'Hères Cedex, France

S. Rolland du Roscoat

Laboratoire Sols-Solides-Structures-Risques (3SR Lab), CNRS/Université de Grenoble (Grenoble INP/UJF), BP 53, 38041 Grenoble Cedex 9, France and European Synchrotron Radiation Facility (ESRF), ID 19 Topography and Microtomography Group, 38043 Grenoble Cedex, France

Synopsis

The non-Newtonian rheology of concentrated fiber suspensions, such as short fiber reinforced polymer composites during their processing, depends on both the microstructure of their fibrous network and the deformation micromechanisms arising at fiber–fiber contacts. In this work, these two aspects are investigated using model concentrated fiber suspensions made up of short glass fiber bundles impregnated in a transparent polymer. For that purpose, multiresolution x-ray microtomography was used to analyze the fibrous microstructures, showing that the studied suspensions exhibit a planar fiber orientation with fairly straight fiber bundles, the connectivity of which can be modeled by the geometrical statistical tube model. Besides, bundle–bundle contact forces together with the interaction between the bundles and the suspending fluid are analyzed by using pull-out experiments. These tests allow the influence of the pull-out velocity, the confining stress and the volume fraction of fiber bundles on the pull-out force to be quantified. Combined with the microstructure analysis, such results are then used to propose a bundle–bundle contact model which can be implemented into multiscale rheological models dedicated to concentrated fiber suspensions. © *2012 The Society of Rheology.* [http://dx.doi.org/10.1122/1.3698185]

[a]Author to whom correspondence should be addressed; electronic mail: Laurent.Orgeas@grenoble-inp.fr

I. INTRODUCTION

Due to their cost efficiency and their very interesting specific physical and mechanical properties, polymer composites reinforced with short fiber bundles such as sheet molding compounds (SMC), glass mat thermoplastics (GMT), and carbon mat thermoplastics (CMT) are extensively used in many applications. These composites have a high volume fraction ϕ of slender fiber bundles (typically ranging from 0.05 to 0.2) with a more or less planar random fiber orientation. Hence, each fiber bundle inside the composite has multiple contact points with its neighbors. This highly affects the physical and mechanical properties of these materials [Osswald and Tseng (1994); Thomasson and Vlug (1996)]. This also drastically affects their rheology during their forming process, i.e., compression molding [Advani (1994); Berglund and Ericson (1995)]. Indeed, during compression molding, such composite materials behave as non-Newtonian and highly concentrated fiber suspensions. They exhibit a complex and not well understood rheology which is significantly affected by bundle–bundle contacts during the suspension flow.

The modeling of the contact micromechanisms constitute one of the key points of multiscale rheological models dedicated to concentrated fiber suspensions [Ausias *et al.* (2006); Djalili-Moghaddam and Toll (2005); Dumont *et al.* (2009); Fan *et al.* (1998); Férec *et al.* (2009a); Joung *et al.* (2001, 2002); Le Corre *et al.* (2004, 2005); Petrich and Koch (1998); Sandstrom and Tucker (1993); Servais *et al.* (1999a, 1999b); Sundararajakumar and Koch (1997); Switzer and Klingenberg (2003); Toll and Månson (1994); Yamane *et al.* (1995)]. In those approaches, fiber suspensions are usually considered as incompressible, and suspending fluids are very often assumed to be Newtonian, even if in most applications suspending fluids exhibit non-Newtonian behaviors [Dumont *et al.* (2003); Ericsson *et al.* (1997); Férec *et al.* (2009b); Gibson and Toll (1999); Le Corre *et al.* (2002); Orgéas *et al.* (2008); Servais *et al.* (1999a, 1999b); Silva-Nieto and Fisher (1981)]. The overall suspension Cauchy stress $\boldsymbol{\sigma}^s$ is often expressed as the sum of various contributions

$$\boldsymbol{\sigma}^s = -p\boldsymbol{\delta} + \boldsymbol{\sigma}^m + \boldsymbol{\sigma}^{fm} + \boldsymbol{\sigma}^{ff}, \tag{1}$$

where the first pressure term $-p\boldsymbol{\delta}$ is associated with the suspension incompressibility, $\boldsymbol{\sigma}^m$ is the extra stress within the suspending fluid, $\boldsymbol{\sigma}^{fm}$ is the fiber stress contribution that takes into account the hydrodynamical interactions between the suspending fluid and the fibers away from fiber–fiber contacts [for the two last stress contributions, see, for instance, Batchelor (1970, 1971); Dinh and Armstrong (1984); Lipscomb *et al.* (1988); Mackaplow and Shaqfeh (1996); Shaqfeh and Fredrickson (1990) in the case of Newtonian suspending fluids and Gibson and Toll (1999); Goddard (1976); Souloumiac and Vincent (1998) for power-law fluids], and where the fiber stress $\boldsymbol{\sigma}^{ff}$ takes into account the mechanical interactions between contacting fibers. In concentrated systems, interactions between contacting fibers are often modeled as Newtonian lubrication forces [Ausias *et al.* (2006); Fan *et al.* (1998); Férec *et al.* (2009a); Joung *et al.* (2002); Sundararajakumar and Koch (1997)]. Other multiscale models have tried to account for more realistic non-Newtonian fiber–fiber interactions such as Coulombic friction and/or nonlinear hydrodynamic friction forces [Le Corre *et al.* (2004, 2005); Servais *et al.* (1999a, 1999b); Switzer and Klingenberg (2003)]. Nonetheless, in this case, because of the very high number of fiber–fiber contacts per unit of volume n_c, the contribution $\boldsymbol{\sigma}^{fm}$ is sometimes neglected with respect to $\boldsymbol{\sigma}^{ff}$ [Caba *et al.* (2007); Le Corre *et al.* (2004, 2005); Servais *et al.* (1999a, 1999b); Toll and Månson (1994)]; such a strong assumption has, however, never been checked experimentally. Anyway, whatever the type of suspending fluid and the type of fiber–fiber interaction, $\boldsymbol{\sigma}^{ff}$ can usually be expressed in the following discrete form:

$$\boldsymbol{\sigma}^{ff} = \frac{1}{V^{\text{rev}}} \sum_{N_c^{\text{rev}}} \mathbf{G_i G_j} \otimes \mathbf{f}^k, \tag{2}$$

where $N_c^{\text{rev}} = n_c V^{\text{rev}}$ is the number of fiber–fiber contacts contained inside a representative elementary volume V^{rev} of the suspension, each contact k between two fibers i and j of centers of mass G_i and G_j inducing a contact force $\mathbf{f}^k$ exerted by the fiber j on the fiber i. The discrete expression (2) of the extra stress tensor $\boldsymbol{\sigma}^{ff}$ reveals the great role of the fibrous microstructure. It also emphasizes the role of contact micromechanisms on the overall rheological behavior of concentrated fiber suspensions.

(1) The fibrous architecture together with the fiber geometry is of first importance. For example, they directly determine the number of fiber–fiber contacts per unit volume n_c (and hence N_c^{rev}), the relative positions $\mathbf{G_i G_j}$ not only of contacting fibers i and j but also the contact surfaces S^k which play a great role on contact forces $\mathbf{f}^k$. So far, some experiments were carried out to analyze the fibrous architectures and their flow-induced evolution in dilute and semidilute systems [Folgar and Tucker (1984); Petrich and Koch (1998); Petrich et al. (2000); Yasuda et al. (2002)]. Conversely, very few experimental studies focused on the characterization of fibrous architectures within the concentrated regime. This clearly hinders both the development and the validation of the micromechanical assumptions of the multiscale rheological models cited previously. For instance, by studying the compression flow of model transparent concentrated fiber bundle suspensions (PMMA + colored glass fiber bundles), Dumont et al. (2007) could analyze the evolution of the bundle orientation, bending, and flattening induced by the suspension flow. However, the results gained in this work were limited because the microstructure characterization was restricted to 2D micrographs. More recent studies tried to overcome such a drawback by using x-ray microtomography, a technique that is now widely used in materials science [Badel et al. (2008); Baruchel et al. (2006); Chalencon et al. (2010); Rolland du Roscoat et al. (2007)]. For example, by using the phase contrast imaging mode, Le et al. (2008) confirmed and refined the results of Dumont et al. (2007) using an industrial compression molded SMC. In particular, the planar orientation of the SMC bundle network was fully characterized, and a significant flattening of bundle was observed during compression molding: despite such bundle flattening should lead to an increase of bundle–bundle contact zones (and hence of contact forces $\mathbf{f}^k$), this latter is not taken into account in current multiscale models. Recently, Latil et al. (2011) performed a compression test of a bundle of aligned fibers saturated by a Newtonian fluid together with in situ 3D characterization of the fibrous network. Not only the position, the orientation, the displacement, and the deformation of each fiber but also the position and the evolution of each fiber–fiber contact were followed during compression. More recently, using again x-ray microtomography, the average number of fiber–fiber contacts per fiber, i.e., the average fiber coordination number $\bar{Z} = 2n_c/n_f$ (n_f being the number of fiber per unit of volume) predicted by the analytical tube model [Doi and Edwards (1978); Le Corre et al. (2005); Ranganathan and Advani (1991); Toll (1993); Vassal et al. (2008)] was recently found to be in a good agreement with that measured in concentrated networks of rather straight copper fibers with circular cross section and planar fiber orientation [Orgéas et al. (2012)]. It could be very interesting to see whether such kinds of elementary microstructure models based upon excluded volume framework [Balberg et al. (1984); Doi and Edwards (1978); Komori and Itoh (1994); Komori and Makishima (1977); Pan (1993); Ranganathan and Advani (1991); Toll (1993)] could be used to describe the

coordination number in suspensions made up of disordered and entangled fiber bundles. Indeed, even if this has never been checked experimentally, many multiscale analytical models of concentrated fiber suspensions use *a priori* the tube model to model the fiber connectivity and to compute the extra stress tensor $\boldsymbol{\sigma}^{ff}$ from Eq. (2) [Alkhagen and Toll (2007); Djalili-Moghaddam and Toll (2005); Férec *et al.* (2009a); Servais *et al.* (1999a, 1999b); Toll (1998); Toll and Månson (1994)].

(2) In order to characterize contact micromechanics between contacting fibers (or fiber bundles), several authors carried out interesting pull-out experiments, which consisted of extracting a straight continuous fiber (or fiber bundle) initially embedded in the fiber suspension. These studies were performed by using not only industrial GMT reinforced by fibers [Servais *et al.* (1999b)] or fiber bundles [Servais *et al.* (1999a)] but also by using CMT [Caba *et al.* (2007)]. These studies are quite complete. For instance, whatever the tested materials, it was observed that the measured pull-out force exhibited a velocity independent yield force at very low pull-out velocities, typically below 10^{-5} m s^{-1}, i.e., below the expected relative velocities $\Delta\mathbf{v}^k$ at the contacts between contacting fibers during industrial compression molding (10^{-5} m s$^{-1} < ||\Delta\mathbf{v}^k|| < 10^{-1}$ m s^{-1}). Above this pull-out velocity, the pull-out force exhibited a noticeable viscous behavior, following power-law [Servais *et al.* (1999b)] or Carreau-Yasuda [Caba *et al.* (2007); Servais *et al.* (1999a)] functions of the pull-out velocity. In all cases, pull-out forces significantly increased with the fiber content ϕ, this increase was directly attributed to the increase of the coordination number $\bar{Z}$ with ϕ. However, these studies did not investigate the influence of a confining stress on contact micromechanisms, although such a confining stress cannot be considered as negligible during compression molding: this point should be explored.

In order to extract contact forces from the pull-out experiments, the friction force the suspending fluid exerts along the continuous bundle outside contacts zones was neglected. As mentioned earlier, this assumption has never been validated experimentally. Besides, contact forces in the former approaches were seen as the sum of three contributions [Servais *et al.* (1999b); Toll and Månson (1994)]: (a) a normal force due to the elastic deformation of the fibrous network [the approach proposed by Servais *et al.* (1999b) and Toll and Månson (1994), the unique source of elastic deformation is the bending of fiber or fiber bundles between contact points], (b) a dry Coulombic friction force induced by the contacts between fibers, and (c) a lubrication force due to shearing of the thin film of suspending fluid separating the fibers in the vicinity of contact zones. Lastly, in order to estimate the number of contacts along the continuous extracted fiber, and hence in order to estimate contact forces, it was again assumed that the fibrous microstructures of the studied suspensions were well described by the statistical tube model. Its relevance remains to be investigated.

Thus, the aim of this study is to complete the aforementioned studies [Caba *et al.* (2007); Servais *et al.* (1999a, 1999b)] to better estimate both the microstructures and contact micromechanisms in concentrated fiber bundle suspensions such as GMT, CMT, or SMC. More precisely, the objective is to bring some answers to the following opened questions. What is the 3D architecture of such fiber suspensions? What is the fiber coordination number? Can it be predicted by an analytical microstructure model such as the tube model? What do contact surfaces look like? What is the nature of contact micromechanisms? Are contact micromechanisms sensitive to the confining stress? Can the role of the suspending fluid far from the contact zones be neglected? For that purpose, model fiber bundle suspensions were processed with various fiber bundle contents and planar random fiber bundle orientation (Sec. II). Their 3D fibrous microstructures were finely characterized by using

x-ray microtomography and dedicated image analysis subroutines (Sec. III). Subsequently, compression and pull-out experiments were carried out using these suspensions at various confining stresses and pull-out velocities (Secs. IV and V). These different results are combined to propose a bundle–bundle contact model (Sec. VI).

II. MATERIALS AND EXPERIMENTAL PROCEDURE

A. Materials

The used suspending fluid is a hydrocarbon gel (Versagel C, Perenco, USA). First, it is transparent: this facilitated the quick observation and the control of the quality of the processed suspensions. Second, at $120\,^{\circ}$C, it behaves as a Newtonian fluid with a very low viscosity of ≈ 1 Pa s; the impregnation and the saturation of the fibrous network during the suspension processing were thus facilitated (see Subsection II B). Third, at room temperature, it behaves as a solid gel, so that the processed suspensions could be easily handled before the experiments, without damaging their microstructures. Lastly, at $50\,^{\circ}$C, its rheology is close to the rheology of matrices used in commercial GMT or SMC formulations. This last point is illustrated in Fig. 1(a), where the steady state shear viscosity of the gel μ at $50\,^{\circ}$C is plotted as a function of the shear rate $\dot{\gamma}$ [the data were obtained on a standard cone-plate rheometer (Anton Paar MCR301), each point being obtained in steady state conditions]. As shown by the continuous line plotted in the graph, data are rather well fitted by a Carreau–Yasuda model, i.e.,

$$\mu = \mu_0 \left(1 + \left(\frac{\dot{\gamma}}{\dot{\gamma}_c} \right)^a \right)^{\frac{n-1}{a}}, \tag{3}$$

where the Newtonian viscosity μ_0, the power-law exponent n, the curvature factor a, and the characteristic shear strain rate $\dot{\gamma}_c$ equal to 27 000 Pa s, 0.4, 2, and 2.10^{-2} s^{-1}, respectively. It has to be emphasized that above shear strain rates of 10–100 s^{-1}, no reliable measurement of the shear viscosity was possible, since the polymer exhibited severe strain localization and the rheometry experiments became heterogeneous.

The fiber bundles which were introduced inside the suspensions were identical to those used in industrial SMC. They were made up of about 200 sized glass fibers having
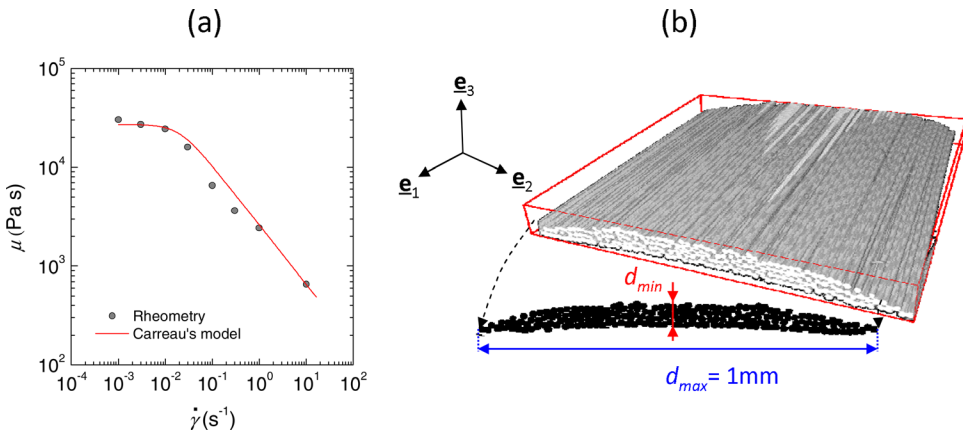
FIG. 1. Materials—(a) Evolution of the steady state shear viscosity μ of the suspending fluid with the shear strain rate $\dot{\gamma}$ at $50\,^{\circ}$C (dots represent the experimental data and the continuous line the Carreau fit). (b) 3D view and cross section of a glass fiber bundle (x-ray microtomography, voxel size $= 0.7\mu$m).

a length of $l = 13$ mm and a diameter $d = 15$ μm. They were processed and sized by Owens Corning Vetrotex Reinforcements (Chambéry, France). As shown from the 3D micrograph displayed in Fig. 1(b), the studied fiber bundles exhibit very flat cross sections, which can be approximated to elliptical cross sections of major axis $d_{max}/2 \approx 0.5$ mm and minor axis $d_{min}/2 \approx 0.1$ mm.

B. Processing of fiber suspensions

The fiber bundle suspensions were processed by following a processing route close to that used by Dumont *et al.* (2007) and Orgéas *et al.* (2012). Briefly, unsaturated preimpregnated homogeneous fibrous networks, with controlled volume fraction ϕ and controlled planar orientation of bundles were first manufactured. Then, these bundle networks were fully impregnated by the suspending fluid. This was achieved inside a heated rectangular mold (surface $S_0 = 165 \times 80$ mm^2) at 90 °C under a compression pressure of 500 Pa for 20 min. The thickness of the as-processed samples was $h_0 = 6$ mm. Samples were processed with five different bundle volume fractions $\phi = 0.08$, 0.1, 0.13, 0.18, and 0.25. Note that in order to perform pull-out experiments (see Subsection II D), five straight continuous, parallel to $\mathbf{e}_1$, fiber bundles were also inserted along the midplane of the suspensions during their processing. Also, note that in order to characterize the rheology of the suspending fluid but also to check the validity of the pull-out tests, samples with the straight continuous and parallel to $\mathbf{e}_1$ fiber bundles immersed in the suspending fluid alone were also processed. Finally, in order to analyze the macroscale rheology of the processed suspensions under (i) drained or dry testing conditions (consolidation tests without suspending fluid or with the suspending fluid at high temperature) or (ii) homogeneous one-phase flows encountered in typical industrial conditions (lubricated compression tests), fiber bundle suspensions and dry fibrous mats were also prepared without any continuous bundle.

C. Imaging of fibrous microstructures

To perform 3D characterization of the fibrous microstructures of the processed suspensions (see Sec. III), x-ray microtomography was used at various spatial resolutions. For that purpose, two different microtomographs were used. For high spatial resolutions, i.e., for voxel sizes of 0.7 and 3.2 μm, the microtomograph of the European Synchrotron Radiation Facility (ESRF, ID19 beamline, Grenoble, France) was used. Scans of small samples cut from the processed suspensions were achieved (overall scanning time $\approx$20 min), consisting of 2700 x-ray 2D radiographs onto a charge coupled device (CCD) detector (2048×2048 pixels) obtained from the incremental rotation of the imaged sample with respect to the synchrotron x-ray source (overall rotation $= 180°$, beam energy $= 34$ keV). For medium spatial resolutions, i.e., for voxel sizes of 15.6 μm, a standard laboratory microtomograph was used (RX Solution apparatus located in 3SR Lab, Grenoble, France). Scans of very large samples could then be achieved (1500 x-ray 2D radiographs onto a 1914×1580 pixels CCD detector, overall rotation $= 360°$, scanning time $\approx$90 min, 100 kV, 140 mA). After suitable reconstruction and image analysis procedures, 3D maps of the x-ray absorption coefficient within each scanned specimen could be obtained [see Fig. 2(a)]. By using a standard thresholding operation (implemented into the software IMAGEJ), it was then possible to obtain 3D binary representations of the fiber bundles [see, for examples, Figs. 1(b) and 2(b)–2(f)].

D. Pull-out experiments

In order to analyze deformation micromechanisms within the processed suspensions, a pull-out device slightly different from those that were previously used [Caba *et al.* (2007); Servais *et al.* (1999a, 1999b)] was designed. The validity of the tests carried out with this
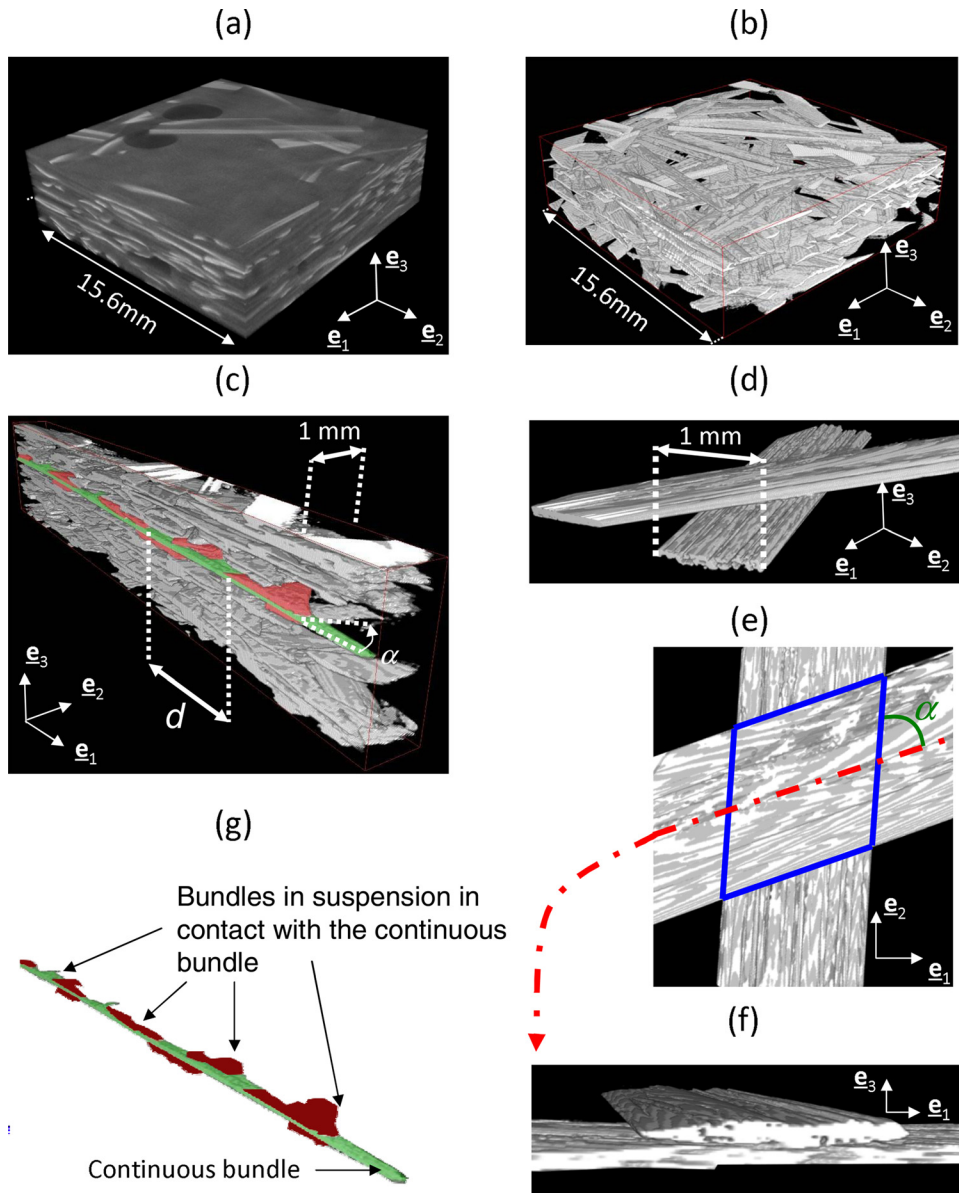
FIG. 2. 3D micrographs obtained from a fiber bundle suspension with $\phi = 0.13$. (a) 3D map of the x-ray absorption coefficient (voxel size 15.6 μm); (b) 3D overview of the fibrous network after thresholding; (c) and (g) 3D views showing the continuous fiber bundle (green) and the short fiber bundles (red) in contact with it; (d)–(f): zooms on a bundle–bundle contact with a 3D view (d), an upper view (e) and a cross section along one of the two fiber bundles (f) (voxel size 3.2 μm).

device is discussed for the suspending fluid and the processed suspensions in Appendices A and B, respectively. Figure 3 depicts the simplified scheme of this apparatus. Briefly, to perform a pull-out experiment, a suspension sample was inserted inside the mold used to process it. The mold is used to contain the suspension flow during the tests. Then, it was heated at 50 °C. Furthermore, the upper rectangular plate of the mold was used to exert a prescribed confining force F_n (or a confining normal stress $\sigma_n = F_n/S_0$) kept constant
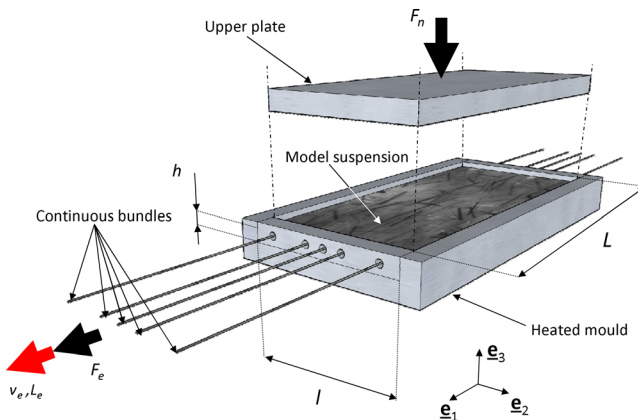
FIG. 3. Scheme of the pull-out apparatus.

during the test. A pull-out experiment consisted of extracting one of the five straight and continuous fiber bundles at a constant pull-out velocity v_e over a pull-out length L_e. This motion was precisely controlled, since the continuous bundle was fastened to the crosshead of a tensile testing machine (MTS 4M). During such an experiment, the pull-out force F_e was recorded using a load cell with a maximum capacity of 60 N. Thereafter, the pull-out force per unit length f_e the tested suspension exerted on the extracted continuous bundle, together with the friction coefficient λ_e could be estimated as

$$f_e = \frac{F_e}{L_e} \quad \text{and} \quad \lambda_e = \frac{f_e}{v_e}. \tag{4}$$

By following this procedure, various tests were achieved for confining stress σ_n and pull-out velocities v_e ranging, respectively, from 0 to 18 000 Pa and from 10^{-5} to 10^{-1} m s^{-1}. Such values correspond to those encountered when processing the considered industrial composites.

E. Macroscale compressions

To analyze the rheology of the suspensions under drained or dry testing conditions or homogeneous one-phase flow situations, consolidation and lubricated compression tests were, respectively, carried out using a dedicated compression rheometer developed in previous studies [Dumont *et al.* (2003); Le Corre *et al.* (2002)]. This rheometer has large dimensions (diameter of the parallel compression plates equal to 400 mm). Thus, it allows the rheological properties of fiber suspensions to be properly characterized, by testing samples with dimensions much larger than the fiber (bundle) length, i.e., without edge effects and with a good scale separation between the sample size and the suspension heterogeneity. This rheometer was mounted onto a MTS 4M mechanical testing machine equipped with a 2 kN load cell. In the case of the consolidation tests (performed using cylindrical samples having an initial diameter 160 mm and a height of 10 mm), the dry fibrous mat and the suspensions were heated at 120 °C. In the case of lubricated compression tests (dimensions of the tested samples 80 mm × 80 mm × 6 mm), the suspensions were heated at 50 °C. In this case, to ensure a homogeneous compression flow, the external surfaces of the samples were lubricated using silicone oil. In both cases, the test was carried out at a constant compression strain rate of 0.1 s^{-1}, whereas the current height h of the sample together with the compression force F were simultaneously recorded.

III. CHARACTERIZATION OF FIBROUS MICROSTRUCTURES

Figure 2 gives a collection of 3D micrographs obtained at various locations inside the processed fiber bundle suspensions (here, with a bundle content $\phi = 0.13$) and various spatial resolutions. Without any further quantitative image analysis, this figure triggers the following comments:

- The 3D overview of the fibrous network in Fig. 2(b) shows that the bundles are well dispersed inside the suspension. Bundles seem to be mainly aligned in the $(\mathbf{e}_1, \mathbf{e}_2)$ plane. This micrograph also shows that the considered suspensions are concentrated so that each bundle has contacts with its neighbors.
- The 3D micrographs displayed in Figs. 2(c) and 2(g) confirm the previous remarks. In addition, these micrographs clearly shows that the continuous bundles which were inserted in the suspension for the pull-out experiments remain straight and parallel to $\mathbf{e}_1$ after the processing phase. These continuous bundles also touch many bundles within the suspensions.
- The visual scrutinization of the volume shown in Fig. 2(b) shows that there are two types of bundle–bundle contacts. A first minor set of contacts is observed between adjacent bundles along their thinnest lateral faces. But the major parts of bundle–bundle contacts look like that represented in the micrographs (d)–(f) in Fig. 2. In this case, contact occurs on the largest lateral surfaces of the bundles. Hence, as the bundles are very flat, the contact zone S^k between two contacting bundles of local bundle orientations $\mathbf{p}^i$ and $\mathbf{p}^j$ [characterized by a local relative angle α, see Fig. 2(e)] can be roughly estimated by a rhomb surface

$$S_k \approx \frac{d_{max}^2}{||\mathbf{p}^i \times \mathbf{p}^j||} \approx \frac{d_{max}^2}{|\sin \alpha|}. \tag{5}$$

- As shown from the various micrographs displayed in Fig. 2, the major axes of the cross section of the bundles mostly lie within the $(\mathbf{e}_1, \mathbf{e}_2)$ plane: this is a direct consequence of the processing route of the bundle suspensions. In the following, we will assume reasonably that all the major axes lay in $(\mathbf{e}_1, \mathbf{e}_2)$.

To get more quantitative data on the fibrous microstructures (e.g., fiber bundle location, tortuosity, orientation, bundle–bundle contact locations, and orientations), the additional image analysis operations were required and achieved using the softwares IMAGEJ and MATLAB. These operations are briefly described below and summarized in Fig. 4. They were performed using two scanned volumes: (i) the volume shown in Fig. 2(b), and (ii) around the continuous fiber bundle displayed in Fig. 2(c).

A. Characterization of fiber bundles

To detect the centerlines of the bundles contained inside the scanned and segmented volumes [i.e., to obtain Fig. 4(b) from Fig. 4(a)], standard 3D skeletonization algorithms (available in commercial image analysis softwares) were first tested and found to be inappropriate. This is essentially due to the very slender geometry of the cross section of the studied bundles. Consequently, the bundle centerlines were detected by using a manual procedure similar to that adopted previously for SMC [Le *et al.* (2008)]. It was then possible to assess the tortuosity of each bundle, defined as the length of the bundle centerline divided by the chord joining the two extremities of the same centerline. Doing so, the average value of the bundle tortuosity is found to be very close to 1 [1.005 in the example given in Fig. 4(b)]. Thus, each fiber bundle i can be considered as straight enough so that
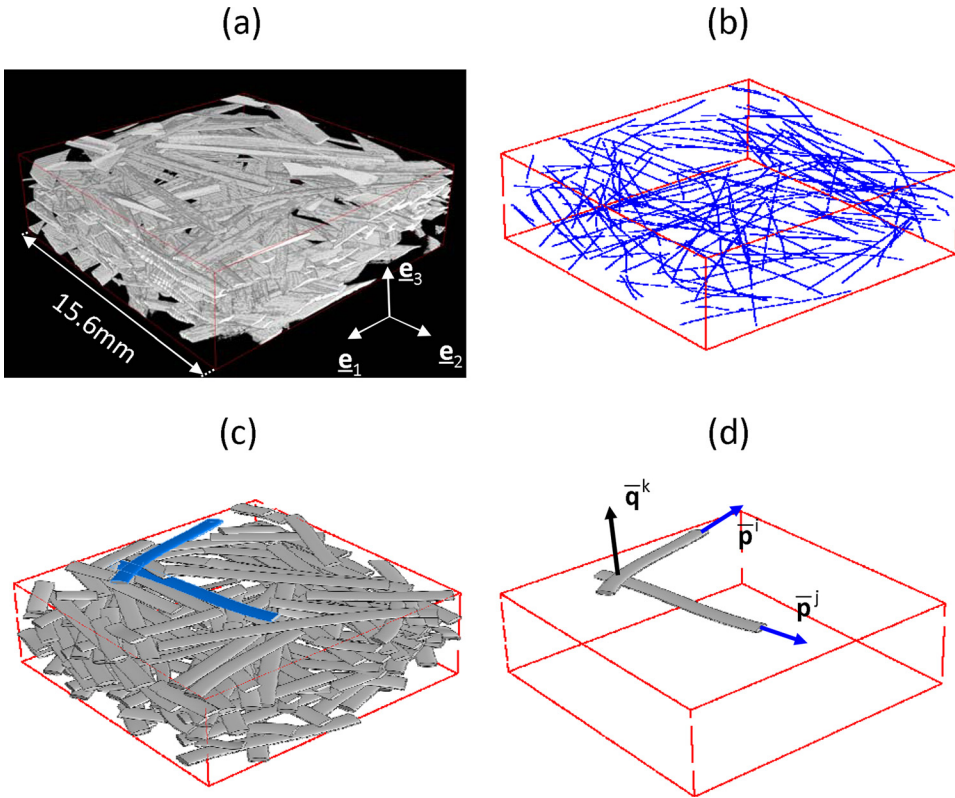
FIG. 4. Method used to estimate fibrous microstructure descriptors. From the segmented volume (a), the bundle centerlines are determined (b), then the bundle network is numerically generated (c) so that the bundle–bundle contacts can be detected (d).

a unique mean orientation vector $\overline{\mathbf{p}}^i$, defined as the unit vector parallel to the minor inertia axis of the considered bundle, can be assigned to it. It is then possible to gauge the bundle orientation in the studied suspensions. This is illustrated in the example of Fig. 5(a), in which two representations of the bundle orientation have been chosen. The first is the richest: the spots plotted on the surface of the unit sphere represent the extremities of the N orientation vectors $\overline{\mathbf{p}}^i$ (the number of bundles N equals 150 in the example given in Fig. 4), their origin being located at the center of the sphere. The second, more compact, is the second order bundle orientation tensors $\mathbf{A}$ [Advani and Tucker (1987)], defined here in its discrete form as [Dumont *et al.* (2007); Latil *et al.* (2011); Le Corre *et al.* (2005); Vassal *et al.* (2008)]

$$\mathbf{A} = \frac{1}{N} \sum_{i=1}^{N} \overline{\mathbf{p}}^i \otimes \overline{\mathbf{p}}^i. \tag{6}$$

As evident from Fig. 5(a), the bundle orientation vectors $\overline{\mathbf{p}}^i$ nearly lie in the midplane $(\mathbf{e}_1, \mathbf{e}_2)$ of the processed planar bundle suspension. Furthermore, a slight preferred orientation is detected in this plane along the $\mathbf{e}_1$-direction.

B. Characterization of bundle–bundle contacts

To get estimations of the coordination number $\overline{Z}$ together with the orientation of bundle–bundle contacts in the studied suspensions, a dedicated algorithm was developed.

(a)

$$A = \begin{bmatrix} 0.62 & -0.00 & -0.01 \\ -0.00 & 0.38 & 0.00 \\ -0.01 & 0.00 & 0.00 \end{bmatrix}_{(\underline{e}_1, \underline{e}_2, \underline{e}_3)}$$

(b)

(c)

$$B = \begin{bmatrix} 0.12 & 0.00 & 0.00 \\ 0.00 & 0.35 & 0.04 \\ 0.00 & 0.04 & 0.53 \end{bmatrix}_{(\underline{e}_1, \underline{e}_2, \underline{e}_3)}$$
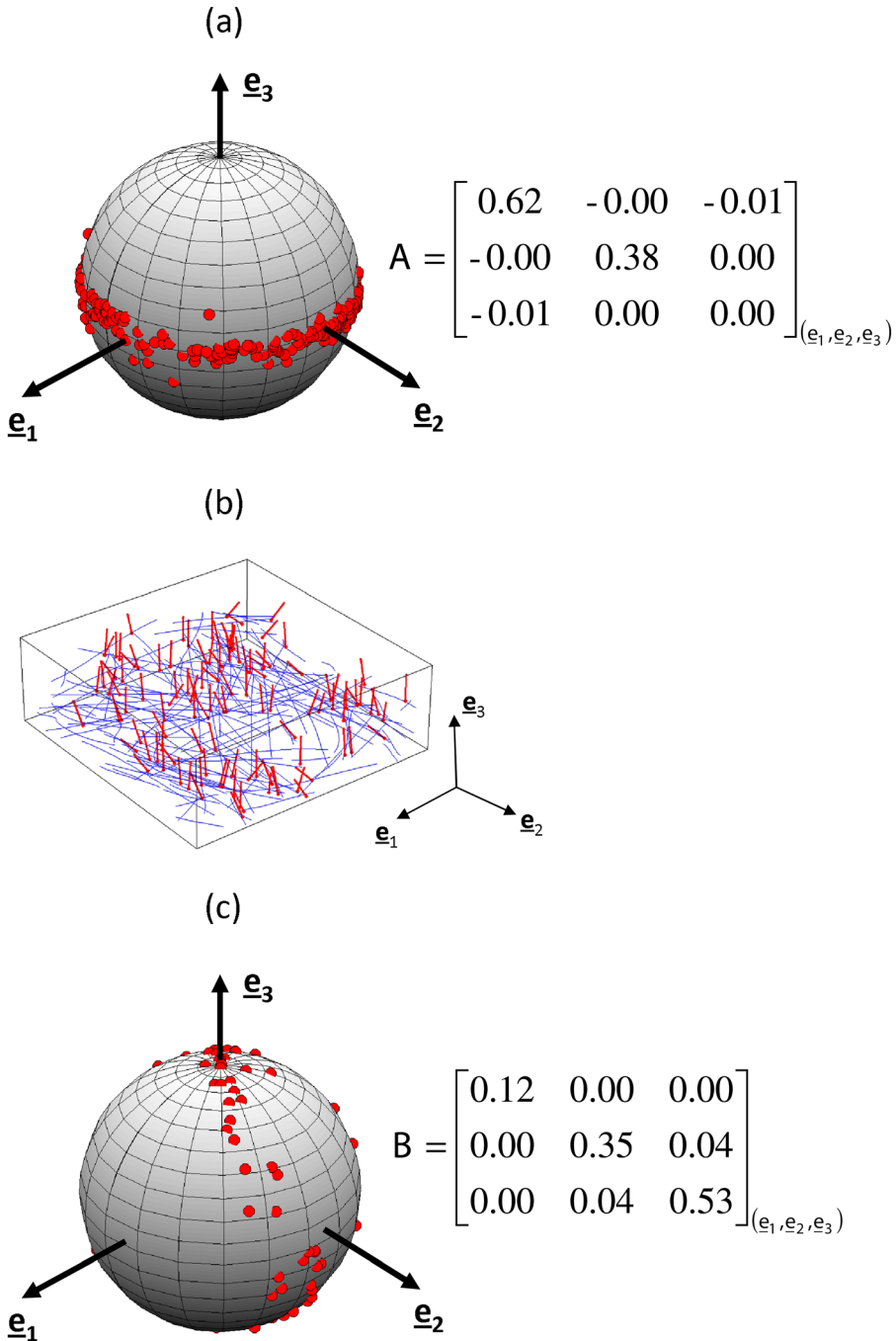
FIG. 5. Orientation of the bundles (a) and of the bundle–bundle contacts (c) in the volume (b).

Thus, from the centerlines of the bundle [see Fig. 4(b)], all the bundles contained in the analyzed volumes were first regenerated numerically, by assuming that they exhibited elliptical cross section (with dimensions d_{max} and d_{min}); this is illustrated in the example given in Fig. 4(c). Then, a contact algorithm was developed to detect the location of the
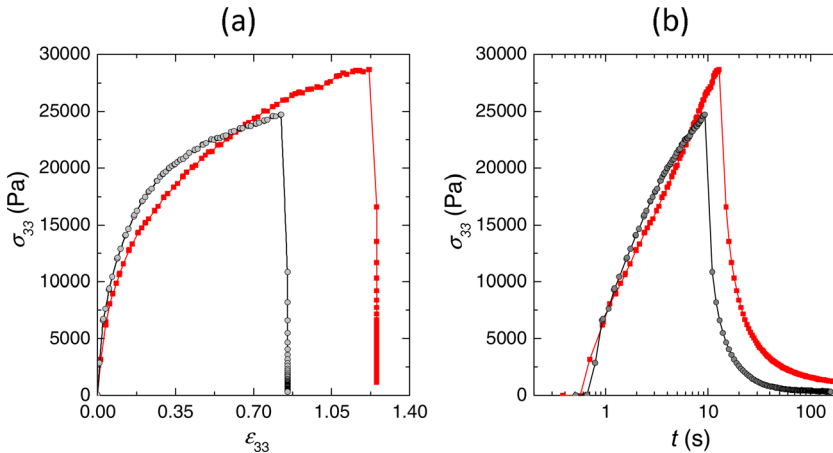
FIG. 6. Stress–strain (a) and stress-time (b) curves recorded during two lubricated simple compressions performed using a suspension with $\phi = 0.13$ at a constant compression strain rate of 0.1 s^{-1} and with two different final compression strains.

$\mathcal{N}$ bundle–bundle contacts (a contact was considered as relevant each time a couple of regenerated bundles overlapped), together with the normal unit vector of each contact k, $\overline{\mathbf{q}}^k$ [see Fig. 4(d)]. An example of results obtained by following this procedure is illustrated in Fig. 5(b). It was then possible to obtain estimations of the average coordination numbers in the studied suspensions. For the example shown in Fig. 4(a), i.e., when $\phi = 0.13$, $\bar{Z}$ reaches 2.9 ± 0.3. The scattering takes into account possible errors induced during the determination of the bundle centerlines [Latil *et al.* (2011)]. This result proves that the studied suspensions belong to the concentrated regime since $\bar{Z} \neq 0$. Similarly, it is found that the number of bundle–bundle contacts per unit length, here noted z, along the continuous bundle shown in Fig. 2(b) is 291 m^{-1}. Next, as for the bundle orientation, it is also possible to analyze the orientation of contacts, either by using a unit sphere representation or the second order orientation contact tensor **B** [Férec *et al.* (2009a); Latil *et al.* (2011)]
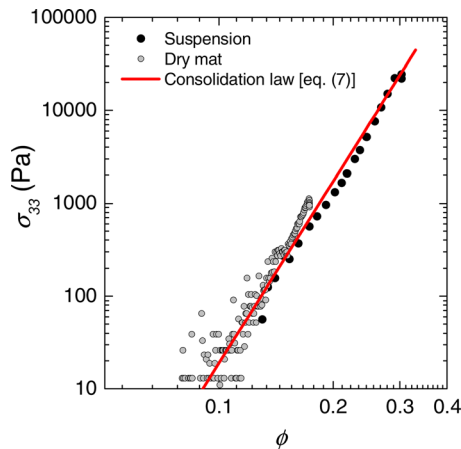
FIG. 7. Evolution of the consolidation stress with respect to the fiber content at a consolidation strain rate of 0.1 s^{-1}. The two sets of data have been obtained with a dry fibrous mat and with the bundle suspension heated at $120°$. The continuous lines represent the fit given by expression (8).

$$\mathbf{B} = \frac{1}{\mathcal{N}} \sum_{k=1}^{\mathcal{N}} \overline{\mathbf{q}}^k \otimes \overline{\mathbf{q}}^k. \tag{7}$$

As shown in the example of Fig. 5(c), most of the normal vectors of bundle–bundle contacts (i.e., those corresponding to the second type previously identified) are orientated along the $\mathbf{e}_3$-direction.

IV. MACROSCALE EXPERIMENTS

A. Lubricated compression experiments

During these experiments, it was first observed that the suspension flow was homogeneous and could be considered as a one-phase plug flow (no fountain flow and no bundle-suspending fluid separation were observed). Besides, measurements of the sample dimensions before and after the tests showed that the flow was practically incompressible (the volume variation being negligible compared with the deviatoric strain the suspensions were subjected to). The graph reported in Fig. 6 shows typical stress–strain and stress-time diagram recorded after two typical tests performed at a compression strain rate of $0.1 \ \mathrm{s}^{-1}$ (the Cauchy compression stress is estimated by assuming the incompressibility of the flow, and the compression strain is the usual Hencky strain). As shown in this figure, a rather good reproducibility of compression curves is observed. Besides, stress–strain curves plotted in graph (a) exhibit a first sharp increase followed by a strain hardening with a lower tangential modulus. Lastly, stress-time curves displayed in graph (b) of this figure show that relaxation curves performed at the end of the compression loading experiments are nearly complete and do not exhibit noteworthy yield stress.

B. Consolidation experiments

For these tests, the packing of the fibrous media occurs without noticeable transverse motion of fiber bundles: the suspending fluid initially saturating the fibrous mats was
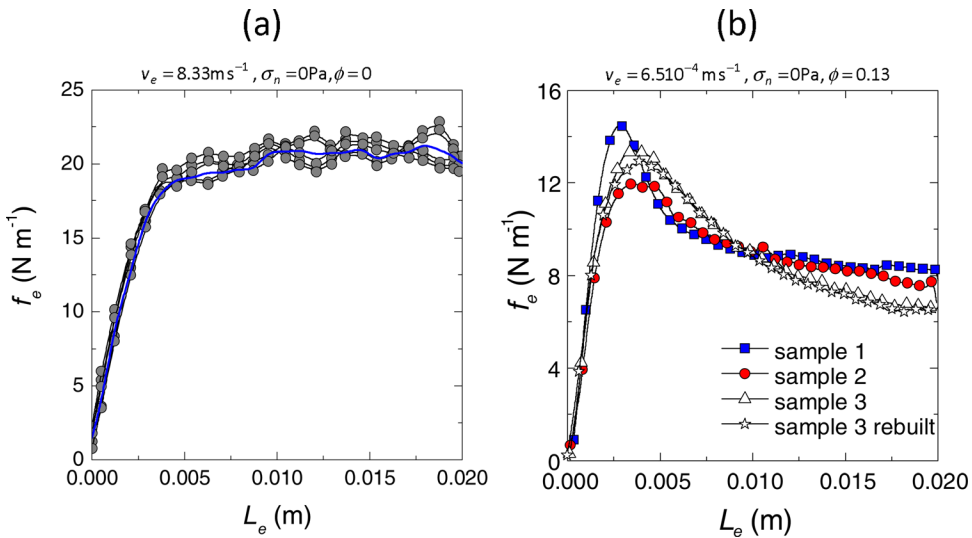

FIG. 8. Typical evolution of the drag force f_e with respect to the pull-out length L_e recorded for the suspending fluid (a) and for the suspension (b). In graph (a), the five experimental curves are obtained by extracting successively the five continuous bundles. In graph (b), they are obtained for different samples and different initial conditions.

expelled from them during the tests. The stress-fiber content diagram plotted in Fig. 7 gives the typical responses recorded during these tests. The two curves which are not very different have been obtained with the dry fibrous mat and with the fiber bundle suspension. As shown from the continuous line plotted in the graph, the two curves can be fitted by a standard power-law type relation which is often proposed for the consolidation of fibrous media [Toll (1998)]

$$\sigma_{33} = k(\phi^m - \phi_0^m), \tag{8}$$

where the stiffness k is close to 60 Pa, the fiber content ϕ_0 reaches 0.077, and where the power-law exponent m is equal to 6.55, i.e., a value similar to those usually observed for such planar random fibrous media [Servais *et al.* (1999a); Toll (1998)]. Lastly, note that the comparison of Figs. 6 and 7 proves that the consolidation stress recorded at $\phi = 0.13$ is much lower than the compression stress observed during lubricated compression experiments at the same fiber content.

V. MICROMECHANICAL EXPERIMENTS

A. Preliminary remarks

The two graphs plotted in Fig. 8 represent the typical evolution of the pull-out force f_e per unit length as a function of the extracted length L_e for the matrix alone (a) and for a suspension with $\phi = 0.13$ (b). In both cases, the confining stress σ_n was zero, and the pull-out velocity v_e was kept constant during the test. The five experimental curves plotted in graph (a) have been obtained with one sample, by extracting successively the five immersed continuous bundles. Obviously, a weak scattering of the results is observed. Thus, in the following, only the averaged value of the five experimental curves will be used, i.e., the blue continuous curve shown in this graph. Besides, the averaged curves plotted in graph (b) have been obtained by using three different suspensions with the same microstructure. Once again, the scattering of the results is rather weak. This implies (i) that the processing route of the suspensions yielded to reproducible samples and (ii) sample dimensions used to perform pull-out tests were large enough to contain enough bundle–bundle contacts on the continuous bundles to be representative. Lastly, the graph (b) also shows that after testing sample 3, it is possible to recover its initial pull-out response by a "healing" treatment which consists of heating the sample at 90 °C for 20 min and cooling it down to the testing temperature.

B. Results

The curves plotted in Figs. 8–10 summarize the behaviors which were observed during the pull-out experiments achieved on the bundle suspensions:

• Figure 8(a) shows that the pull-out force f_e per unit length for the suspending fluid rapidly increases in the beginning of the test (due to the viscoelasticity of the suspending fluid) and reaches a steady state horizontal plateau f_{ep} that only depends on the pull-out velocity v_e. To illustrate this, the friction coefficient at the plateau λ_{ep} is plotted in Fig. 10(b) as a function of the pull-out velocity v_e. The evolution of λ_{ep} exhibits two stages: first, at low pull-out velocities, the friction coefficient tends to be a constant value, and second, at high pull-out velocities, the friction coefficient is a decreasing function (in power-law) of v_e, the exponent of which is equal to 0.4, i.e., that reported during the cone-plate experiments (see Fig. 1 and Appendix A).
• For the suspensions, usually, after a rapid increase of the pull-out force per unit length
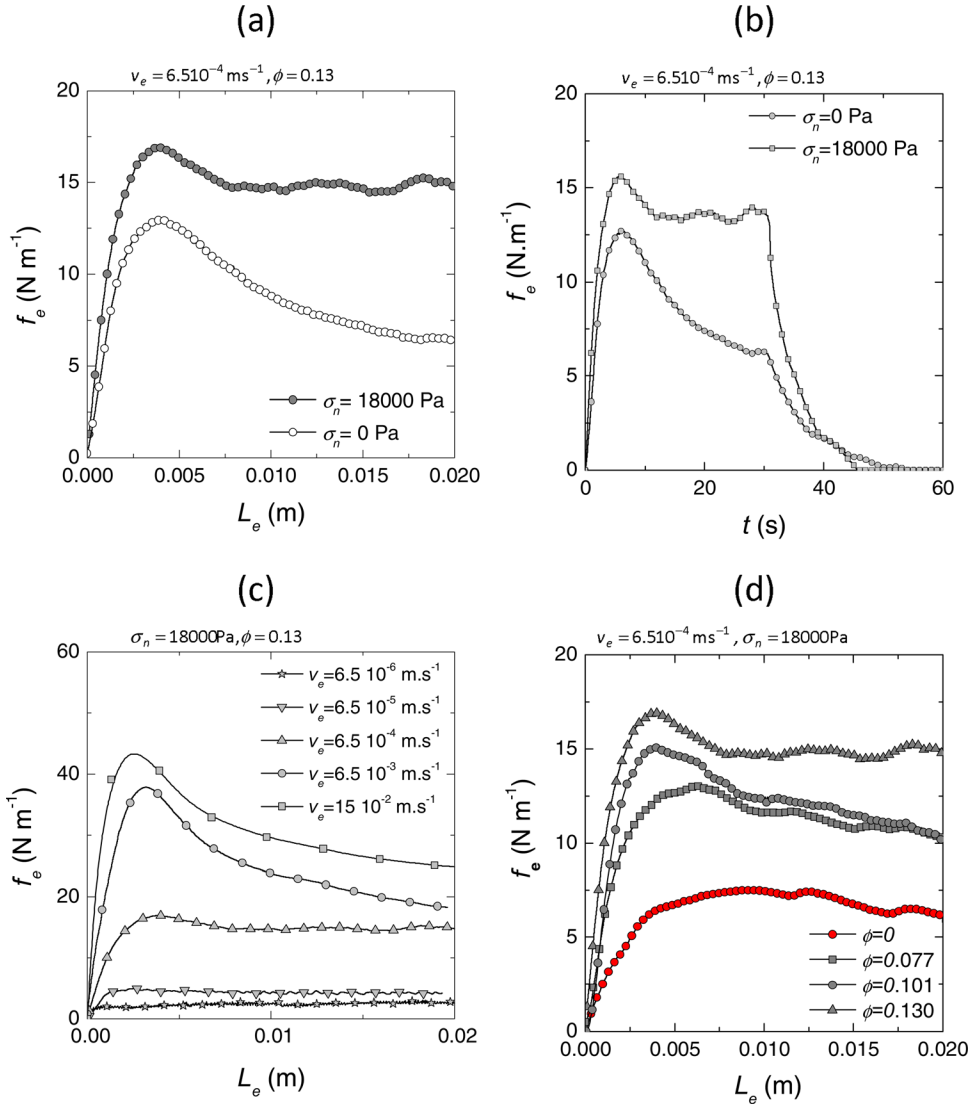
FIG. 9. Evolution of the pull-out force f_e in various testing conditions. (a): $f_e - L_e$ curves showing the influence of the confining stress σ_n. (b) Same tests but with $f_e - time$ graph. (c) and (d): $f_e - L_e$ curves showing the influence of the pull-out velocity v_e and the fiber content ϕ, respectively.

f_e, similar to that observed in Fig. 8(a) for the suspending fluid, a decrease of f_e is observed after a peak f_{ep}, see, for instance, Figs. 8(b), 9(a), and 9(b). Such a decrease is more and more pronounced as the fiber content increases. It is related to the damage of the matrix within bundle–bundle contact zones, where shear strains and shear strain rates are very high (see remarks stated in Subsection II A for the suspending fluid rheology). Depending on the test conditions, such a decrease can be more or less pronounced. Indeed, it can be hindered and can even disappear (i) as the confining pressure σ_n is increased, as shown in Figs. 9(a) and 9(b) and/or (ii) as the pull-out velocity v_e is decreased, as evident in Fig. 9(c).

• Whatever the confining stress σ_n, fiber content ϕ, extracted length L_e, and pull-out velocity v_e, relaxation curves recorded at the end of tests exhibit no residual force. This is
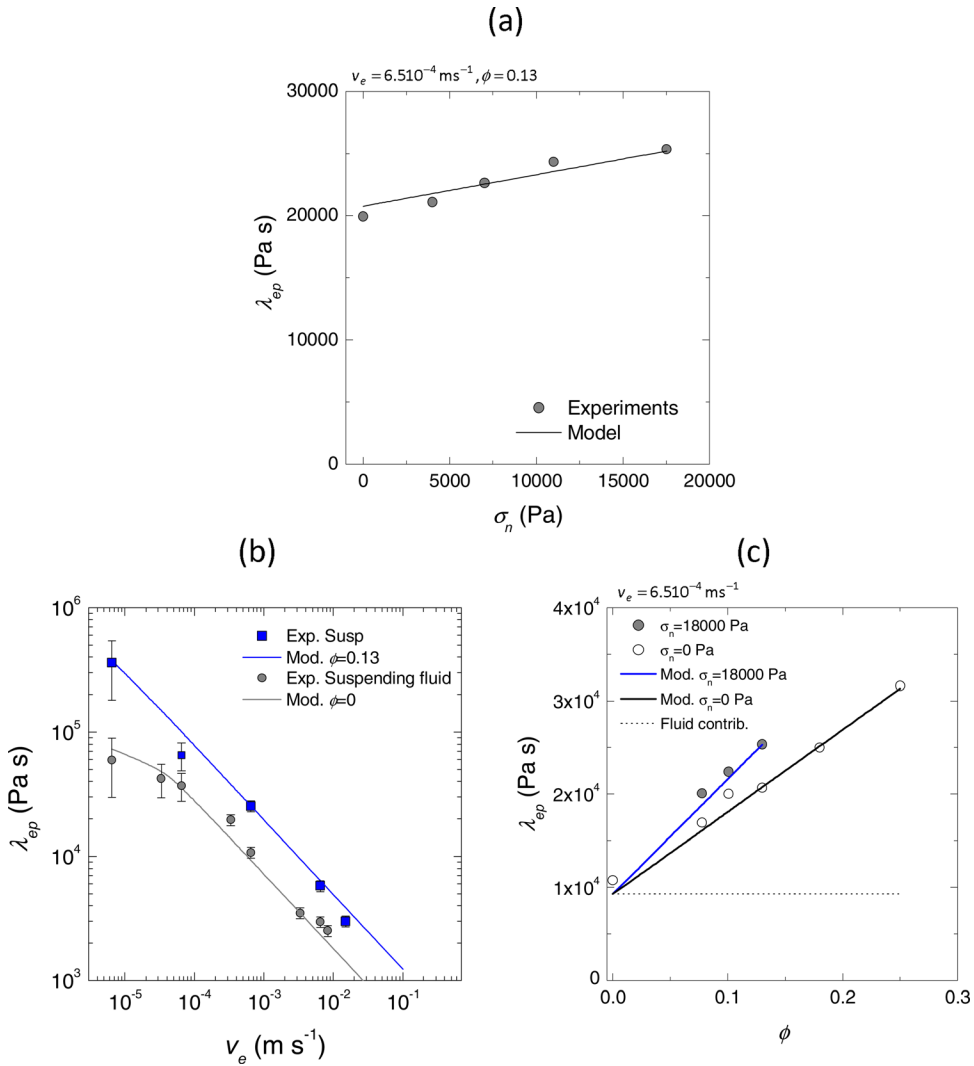
FIG. 10. Evolution of the drag coefficient λ_{ep} with the confining stress σ_n (a), the pull-out velocity v_e (b) and the fiber content ϕ (c). Continuous lines are the predictions given by the proposed pull-out model.

illustrated with the two curves plotted in Fig. 9(b), where f_e falls rapidly down to zero after the end of the pull-out tests, i.e., after 30 s.

- As shown in the graphs (a) and (b) of Fig. 9, the confining stress curbs the decrease of the f_e after f_{ep}. Furthermore, it also increases pull-out force levels. To illustrate this more precisely, we have plotted in Fig. 10(a) the evolution of the friction coefficient recorded at the peak force, i.e., $\lambda_{ep} = f_{ep}/v_e$, with the confining stress σ_n. This graph shows the nearly affine increase of λ_{ep} with σ_n. For example, when $\phi = 0.13$ and $v_e = 6.510^{-4}\,\mathrm{m\,s^{-1}}$, the drag coefficient is subjected to an increase of approximately 35% when the confining stress goes from 0 to 18 000 Pa.

- Figure 9(c) also reveals the strong and major influence of the pull-out velocity v_e on the pull-out the force per unit length. This point is further emphasized in Fig. 10(b), where the evolution of λ_{ep} with v_e has been plotted. As evident from this graph, $\lambda_{ep}(v_e)$ nearly follows a power-law, i.e., $\lambda_{ep} = \lambda_0 v_e^{n-1}$. It is important to mention that the

exponent n of this power-law is equal to 0.4, i.e., the value found for the suspending fluid at high shear strain rates (see Fig. 1).

- As underlined in Fig. 9(d), the higher the fiber content ϕ, the higher the pull-out force, and the stiffer the pull-out response. This is more precisely illustrated in Fig. 10(c): whatever the confining stress σ_n, the friction coefficient λ_{ep} is an affine function of the fiber content ϕ. For instance, when $\sigma_n = 0\,\mathrm{Pa}$ and $v_e = 6.510^{-4}\,\mathrm{m\,s^{-1}}$, an approximately 200% increase of λ_{ep} is recorded as the fiber content ϕ goes from 0 to 0.25. Lastly, please note that the friction coefficient λ_{ep} of the matrix alone ($\phi = 0$) is of the same order of magnitude than those recorded for the bundle suspensions.

VI. DISCUSSION

A. Comments on the fibrous microstructures

The 3D micrographs obtained from x-ray microtomography and their associated image analysis subroutines bring very useful data on the fibrous architectures of the studied fiber bundle suspensions. These data can greatly contribute to build relevant representations of the stress tensors involved in Eq. (1). The following points illustrate this idea:

- By using the discrete representation of the suspension [e.g., Fig. 5(b)], it is possible to obtain 3D data about the geometry, position, and orientation of fiber bundles. In our case, fiber bundles can be approximated as straight cylinders. This observation is in accordance with most of the multiscale rheological models dedicated to suspensions made up of rigid fibers. For fiber bundles, if this assumption may be questionable in some severe flow conditions [Le *et al.* (2008); Odenberger *et al.* (2004)], it remains valid and reasonable in most flow situations [Dumont *et al.* (2007); Le *et al.* (2008)]. Hence, it is then possible to get 3D discrete estimations, e.g., from Fig. 5(a), of the fiber orientation distribution function ψ which is widely used in analytical rheological models for semidilute or concentrated fiber suspensions (see the references cited in the Introduction). In the case of Newtonian suspending fluids and linear fiber–fiber interactions, it is also possible to estimate the fourth order fiber orientation tensor $\mathbb{A}$ [Advani and Tucker (1987)] usually involved in analytical expressions of $\boldsymbol{\sigma}^{fm}$

$$\mathbb{A} = \frac{1}{N} \sum_{i=1}^{N} \overline{\mathbf{p}}^i \otimes \overline{\mathbf{p}}^i \otimes \overline{\mathbf{p}}^i \otimes \overline{\mathbf{p}}^i, \tag{9}$$

together with the fourth order interaction tensors $\mathbb{B}$ introduced in some recent analytical forms of $\boldsymbol{\sigma}^{ff}$ in the case of linear fiber–fiber interactions [Djalili-Moghaddam and Toll (2005); Férec *et al.* (2009a, 2009b)]

$$\mathbb{B} = \frac{1}{N^2} \sum_{i=1}^{N} \sum_{j=1}^{N} ||\overline{\mathbf{p}}^i \times \overline{\mathbf{p}}^j|| \overline{\mathbf{p}}^i \otimes \overline{\mathbf{p}}^i \otimes \overline{\mathbf{p}}^i \otimes \overline{\mathbf{p}}^i. \tag{10}$$

- The present method also allows the locations and the number of bundle–bundle contacts in the suspensions to be estimated, showing that they belong to the concentrated regime, the average coordination number being far from zero. As mentioned in the Introduction, it may be very useful to see whether the as-determined bundle connectivity can be approached by simple analytical expressions such as the very simple and widely used tube model. Basically, the tube model assumes (i) that fibers are straight, homogeneously distributed in space, and (ii) that fibers can overlap (soft core assumption). It proposes an estimation of the average coordination number $\bar{Z}$ in the case of fibers with identical circular cross section of diameter d and identical length l, from the knowledge of the fiber content ϕ and orientation

$$\bar{Z} = 4\phi \left(\frac{2}{\pi} \frac{l}{d} \Phi_1 + \Phi_2 + 1 \right). \tag{11}$$

Similarly, the number of fibers per unit length z intersecting a straight and continuous fiber of the same diameter, orientated along the $\mathbf{e}_1$-direction and immersed within the same suspension is estimated as

$$z = \frac{4\phi}{l} \left(\frac{2}{\pi} \frac{l}{d} \phi_1 + 1 \right). \tag{12}$$

In the above two expressions, the functions Φ_1, Φ_1 and ϕ_1 only depend on the fiber orientation. They can be estimated by the following discrete forms:

$$\begin{cases} \Phi_1 = \frac{1}{N^2} \sum\limits_{i=1}^{N} \sum\limits_{k=1}^{N} \|\bar{\mathbf{p}}^i \times \bar{\mathbf{p}}^k\|, \\ \Phi_2 = \frac{1}{N^2} \sum\limits_{i=1}^{N} \sum\limits_{k=1}^{N} |\bar{\mathbf{p}}^i \cdot \bar{\mathbf{p}}^k|, \\ \phi_1 = \frac{1}{N} \sum\limits_{i=1}^{N} \|\bar{\mathbf{p}}^i \times \mathbf{e}_1\|. \end{cases} \tag{13}$$

By using the x-ray microtomography, we have recently obtained some experimental results to assess the relevance of this model for concentrated fibrous media made up of rather straight fibers with circular cross section. When the fibrous media exhibited planar fiber orientation with fibers randomly or slightly aligned in the suspension midplane, the tube model seems to provide a good prediction [Orgéas *et al.* (2012)]. When the fibers are aligned, the tube model may be inappropriate [Latil *et al.* (2011)]. In the particular case of fiber bundles exhibiting elliptical cross sections and planar orientations, it is possible to revisit and recast the above expressions, which remain valid by simply replacing d by d_{max}. Thus, Eqs. (11) and (12) show that the predicted coordination numbers $\bar{Z}$ and z are linear functions of the fiber bundle content ϕ and that $\bar{Z}$ is an affine function of the fiber bundle aspect ratio l/d_{max}. From the knowledge of the microstructure descriptors obtained in Sec. III (geometry, content, and orientation of fiber bundles), the predicted values of $\bar{Z}$ and z are found to be equal to 3.0 and 285 m^{-1}, respectively. These predictions are fairly close to the experimental values of 2.9 and 291 m^{-1} directly found from the 3D micrographs shown in Fig. 2. Even if this result has to be further validated with other similar fibrous microstructures, it tends to prove that the tube model is able to capture correctly the coordination numbers of the studied fiber bundle suspensions. The consequences of this result are twofold. First, it gives strength and relevance to the rheological models developed using similar microstructure assumptions to propose representations for the stress contribution $\boldsymbol{\sigma}^{ff}$ [Djalili-Moghaddam and Toll (2005); Férec *et al.* (2009a); Le Corre *et al.* (2005); Servais *et al.* (1999a, 1999b); Toll and Månson (1994)]. Second, the pull-out experiments detailed in Sec. V can be analyzed without strong *a priori* assumptions on the coordination number z (see Subsection VI B).

• As shown in Fig. 5, the orientation of the fiber bundles is essentially planar, the major axes of the cross section of the bundles lying in the principal orientation plane ($\mathbf{e}_1, \mathbf{e}_2$). This particular orientation induces fiber bundle contacts (i) mainly orientated along the $\mathbf{e_3}$-direction and (ii) with rhomb-shaped contact surfaces that can be estimated from the simple knowledge of the relative orientation of contacting bundles, as emphasized in Fig. 4. The first point is in accordance with models dedicated to planar fiber

suspensions [Dumont *et al.* (2009); Le Corre *et al.* (2004, 2005); Servais *et al.* (1999a, 1999b); Toll (1998); Toll and Månson (1994)]. The second point is in accordance with the assumptions stated in the micromechanical model proposed by Le Corre *et al.* (2005) in order to estimate the tangential components of contact forces $\mathbf{f}^k$ involved in Eq. (2).

B. Comments on the pull-out experiments

The trends emphasized in Figs. 9 and 10 can also be commented as follows:

- In previous studies dedicated to the experimental analysis of contact mechanisms within concentrated fiber or fiber bundle suspensions [Caba *et al.* (2007); Servais *et al.* (1999a, 1999b)], a yield pull-out force was observed both during constant pull-out velocity experiments (at low velocities) and relaxation tests. Such a yield pull-out force was sometimes dominant [Servais *et al.* (1999b)] or of the same order of magnitude than the viscous part of the pull-out force. It was related to dry Coulombic forces between contacting fibers or fiber bundles. According to the authors, the resulting dry contact forces induce a macroscopic yield stress when the suspension is deformed: this was confirmed by the macroscopic rheological measurements they performed. The results obtained in this work do not follow this trend. Indeed, the typical relaxation curves plotted in Fig. 9(b) and the evolution of the pull-out friction coefficient λ_{ep} shown in Fig. 10(b) prove that the flow micromechanisms arising along the extracted continuous bundle induce no noticeable yield pull-out force, at least for the tested conditions which are close to those encountered in industrial conditions; relaxation curves are complete and the function $\lambda_{ep}(v_e)$ is a power-law with an exponent equal to -0.6, i.e., the value found for the suspending fluid alone at high shear strain rates [see Fig. 1(a)] or high pull-out velocities [see Figs. 12(a) and 10(b)]. Hence, by reasonably assuming the following decomposition of the pull-out force per unit length f_e

$$f_e = f_e^m + f_e^f, \tag{14}$$

the interaction forces per unit length f_e^m and f_e^f the matrix and the contacting bundles, respectively, exert on the extracted continuous bundle are proved to be mostly of visco-elastic type for the studied fiber bundle suspensions. If this seems obvious for the contribution f_e^m, then this implies that the contact contribution f_e^f may be mainly related to nonlinear hydrodynamic lubrication forces induced by the deformation of the suspending fluid entrapped within contact zones. This idea is in agreement with some of the micromechanical assumptions stated in multiscale models [Le Corre *et al.* (2004, 2005); Servais *et al.* (1999a, 1999b); Toll and Månson (1994)]. As a direct consequence, the studied suspensions should exhibit a macroscopic rheology with dominant fluidlike behavior [Le Corre *et al.* (2004)]. As shown in Fig. 6, this trend is confirmed; stress relaxation curves performed after the constant strain rate loading do not show any significant yield stress [notice that this fluidlike rheology was already observed with some GMT or SMC in Ducloux *et al.* (1992); Dumont *et al.* (2003, 2007); Gibson and Toll (1999); Le Corre *et al.* (2002)].

- In order to study the influence of the fiber content ϕ on the pull force, Servais *et al.* (1999a, 1999b) and Caba *et al.* (2007) packed the fibrous media of their suspensions under dry or drained conditions. The induced packing stresses increased both contact surfaces and normal contact forces. The increase of the normal contact forces was related to the out-of-plane bending of fiber bundles during the packing [Toll (1998); Toll and Månson (1994)]. Such normal contact forces induced in turn tangential dry Coulombic forces observed during their pull-out experiments. The present experiments

were carried out using different testing conditions. They complete the aforementioned studies. Indeed, in our case, once the studied suspensions are packed during their initial processing phase (Sec. II), they are not packed any longer. Instead, during the pull-out experiments, they are subjected to an additional macroscopic confining stress σ_n under undrained testing conditions and at nearly constant volume (by assuming the incompressibility of the suspensions). Thus, at the bundle scale, the deformation of the bundle network is expected to be negligible, even in the presence of σ_n which essentially acts as a confining pressure p. However, as underlined in Fig. 10(a), a non-negligible increase of λ_{ep} with σ_n is observed. Hence, the origin of this trend may be due to other pressure-induced micromechanisms occurring within bundle–bundle contact zones, such as the diminishing of the thickness of the entrapped suspending fluid or the enlarging of the bundle width in contact zones, the last mechanism was already observed during lubricated compression [Dumont *et al.* (2007)] or compression molding [Le *et al.* (2008)]. Unfortunately, at the moment, it is not possible to observe such microstructure changes using microtomography; scanning large samples subjected to a confining stress, at a sufficient spatial resolution to observe such deformation micromechanisms, are currently not available.

- Microtomography measurements have shown that the tube model can reasonably predict coordination numbers z and $\bar{Z}$ in the studied fiber bundle suspensions. In particular, at constant bundle orientation, the tube model predicts a linear increase of the coordination number z of the extracted continuous bundle with respect to the fiber content ϕ, as underlined from Eq. (12). Thus, this implies that, in the concentrated regime, the contribution f_e^f probably increases more or less linearly with the fiber content too. From both this result and the tendencies shown in Fig. 10(c), this also implies that f_e^m is either constant or an affine function of ϕ, at least for the tested conditions shown in this graph. In Figs. 10(a) and 10(b), note that the friction coefficient of the matrix alone is of the same order of magnitude than those obtained for the suspensions. Thus, this also proves that f_e^m should not be neglected compared to f_e^f. This is not in agreement with the micromechanical assumptions stated in some of the pull-out or suspension models of the literature [Caba *et al.* (2007); Le Corre *et al.* (2005); Servais *et al.* (1999a, 1999b); Toll and Månson (1994)].

C. A pull-out model

From the experimental results and the previous discussion, a pull-out model is now proposed to estimate the contributions f_e^m and f_e^f. This model is built upon two main hypotheses. First, as revealed in Subsection VI A, the geometrical statistical tube model is supposed to be relevant to describe the bundle structure. Second, as underlined in Subsection VI B, no significant yield force is observed so that it is assumed that the pull-out force is induced by fluidlike interaction forces. Within this framework and for the sake of simplicity, the model focuses only on peak forces by assuming purely viscous flow mechanisms at the bundle scale.

1. Estimation of f_e^m

To estimate the force per unit length f_e^m, the numerical procedure used to check the validity of the pull-out test in the case of the suspending fluid (see Appendix A and Fig. 12) was adapted to the case of the concentrated bundle suspensions, by taking advantage of the 3D micrographs shown in Fig. 2. More precisely:

- Within zones that were located between bundle–bundle contacts [see Fig. 11(a)], orthogonal slices to the continuous bundle were extracted from the 3D micrographs [three per zone, see the examples shown in Fig. 11(a)]. On each slice, the boundary value problem
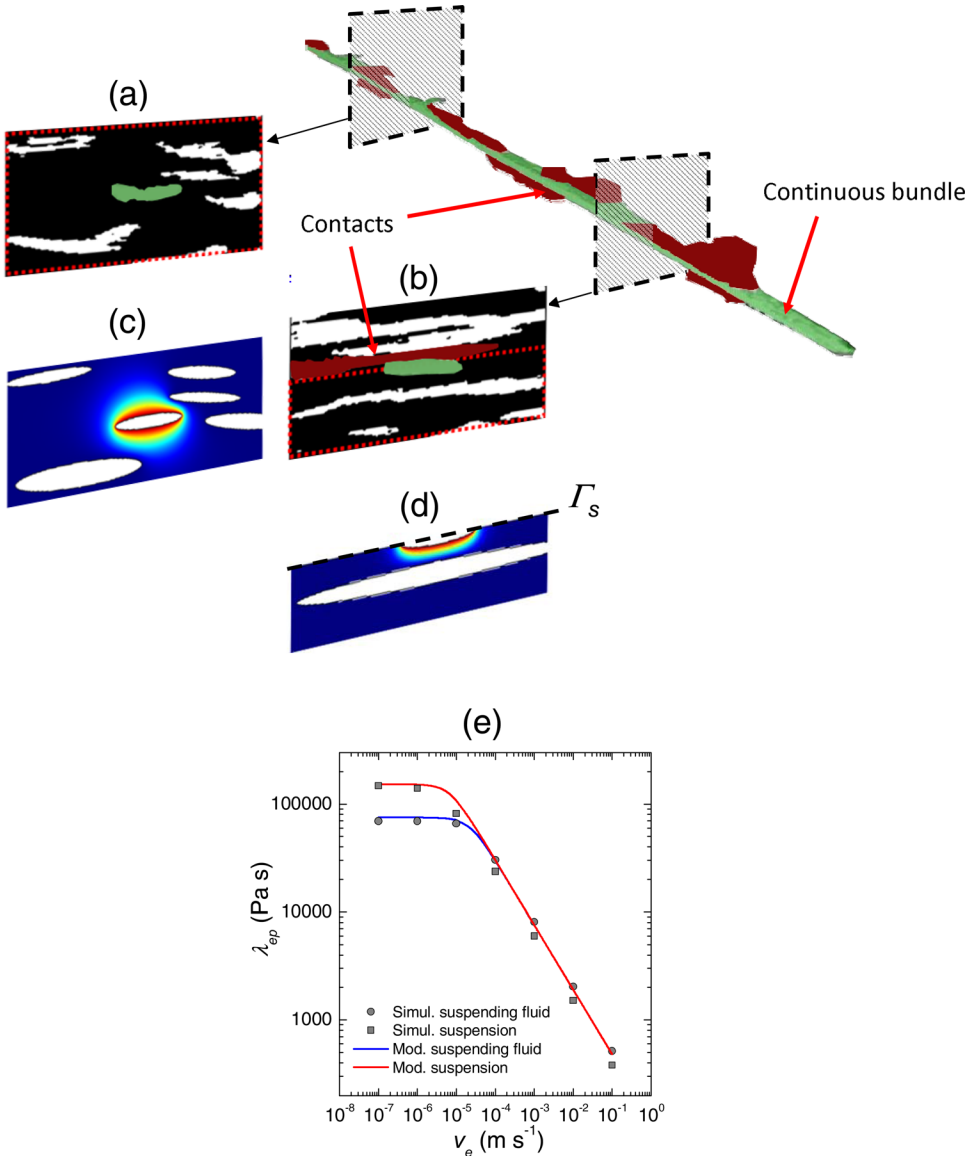
FIG. 11. Method used to estimate f_e^m for $\phi = 0.13$. (a) and (b) Along the continuous bundle, orthogonal slices were extracted from 3D micrographs. (c) and (d) Slice idealization used to run the FEM calculations. In the case where slices are located in a bundle–bundle contact zone (d), only the half space was modeled and a symmetry condition was set on Γ_s. Color maps given in (c) and (d) represent the norm of the velocity field ranging linearly from zero (blue) to v_e (red). (e) Evolution of the computed drag coefficient λ_e^m with v_e (marks) and fits of Eq. (15) used to capture numerical results (continuous lines).

  (A1) was solved (i) by idealizing the sections of fiber bundles as ellipses [see Fig. 11(c)] and (ii) by updating the surface Γ of problem (A1) to impose a zero velocity field on the external surfaces of the bundles surrounding the extracted continuous bundle.

• Within zones that were located above or below bundle–bundle contacts [see Fig. 11(b)], the same procedure was followed. However, in these cases only the half spaces above or below contacts were considered, and a symmetry boundary condition was added on the surface Γ_s [see Fig. 11(d)].
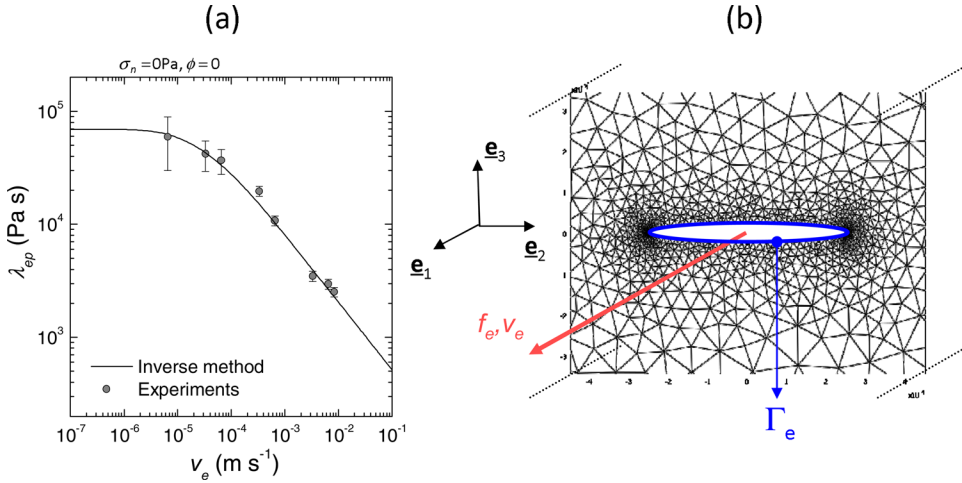
FIG. 12. Evolution of the drag coefficient λ_{ep} with v_e for the suspending fluid (a). The continuous line shown in this graph is the best fit obtained by an inverse modeling that used a direct FE calculation: a zoom of the corresponding P2-P1 mesh around the cross section of the extracted bundle is shown in (b).

- Then, for each zone, the three calculations were averaged and used to compute the friction force per zone, the sum of these friction forces being finally normalized by the total length of the scanned sample in order to get an estimation of the friction force per unit length f_e^m.

Such an estimation is not as precise as a full 3D calculation that would have been heavy and difficult to perform, in particular, due to discontinuities in contact zones and to the very high degrees of freedom it would have required to run such nonlinear calculations with reasonable accuracy. Nonetheless, it should capture the main trends of the nearly unidirectional flow surrounding the continuous bundle during its extraction. At the same time, it is expected to give more accurate results than analytical forms which could have been developed based on micromechanical cell approaches usually dedicated to semidilute suspensions [Batchelor (1971); Goddard (1976); Souloumiac and Vincent (1998)]. Note that these approaches are not appropriate for the considered concentrated suspensions, since they were developed for semidilute systems and/or for power-law suspending fluids.

The results deduced from the numerical analysis are displayed in Fig. 11(e). This figure shows that the resulting friction coefficient λ_e^m exhibits a Carreau-like response with a Newtonian plateau (i) higher than that recorded for the suspending fluid alone and (ii) occurring at pull-out velocities lower than those obtained for the suspending fluid. These two trends are associated with two competitive phenomena: (i) the presence of neighboring bundles that restrain the flow of the suspending fluid and increase local shear strain rates, (ii) the diminishing of the contact surfaces between the suspending fluid and the continuous bundle due to the presence of bundle–bundle contacts. At high pull-out velocities, $\lambda_e^m(\phi = 0.13)$ is surprisingly slightly below but nearly identical to $\lambda_e^m(\phi = 0)$: the first mentioned phenomenon is diminished because of the high shear thinning of the suspending fluid that restrains sheared zones in the vicinity of the continuous extracted bundle [Souloumiac and Vincent (1998)]. Thus, from the numerical results obtained in the cases where $\phi = 0$ (see Appendix A) and $\phi = 0.13$, the following phenomenological analytical equation of f_e^m is then proposed:

$$f_e^m = \lambda_e^m v_e = \lambda_{e0}^m (1 + \beta\phi) \left(1 + (1 + \beta\phi)^{\frac{-2}{n-1}} \left(\frac{v_e}{v_{c0}} \right)^2 \right)^{\frac{n-1}{2}} v_e. \qquad (15)$$

The last expression involves only three constitutive parameters: λ_{e0}^m and v_{c0}, set, respectively, to $75\,000$ Pa s and 2.2×10^{-5} m s^{-1} from pull-out experiments carried out with the suspending fluid alone, and β, found to be equal to 8. Keeping in mind that an *a priori* evolution was chosen in Eq. (15) for fiber contents ϕ comprised between 0 and 0.13 (this has to be validated in future work), Fig. 11(e) shows that such a phenomenological model gives a correct fit of numerical results.

2. Estimation of f_e^f

As proposed by Servais *et al.* (1999a) and Le Corre *et al.* (2005), the very complex shear occurring inside a given contact zone during the relative motion of two contacting bundles is supposed to be equivalent to the simple shear of an equivalent thickness e of the suspending fluid at an equivalent shear rate $\dot{\gamma} = v_e/e$. For simplicity, it is then further assumed that (i) the thicknesses of contact zones rather close to their mean value $\bar{e}$ and (ii) the shear viscosity of the suspending fluid obeys to a Carreau's law [see Fig. 1 and Eq. (3)]. Thus, the contact force contribution f_e^f can be expressed as

$$f_e^f = z\bar{f}^f. \qquad (16)$$

The averaged contact force $\bar{f}^f$ involved in the last equation is written as

$$\bar{f}^f = \bar{S}\mu_0 \left(1 + \frac{p}{p_0} \right) \left(1 + \left(\frac{1}{\dot{\gamma}_c} \frac{v_e}{\bar{e}} \right)^2 \right)^{\frac{n-1}{2}} \frac{v_e}{\bar{e}}, \qquad (17)$$

where $\bar{S}$ represents the averaged contact surface and depends on the relative orientations of contacting bundles with respect to the continuous bundle. From the geometry of contact zones [see Figs. 2(d)–2(f) and Eq. (5)], $\bar{S}$ can be estimated by the following equation:

$$\bar{S} = d_{max}^2 \phi_1', \quad \text{where} \quad \phi_1' = \frac{1}{N} \sum_{i=1}^{N} \frac{1}{||\bar{\mathbf{p}}^i \times \mathbf{e}_1||}, \qquad (18)$$

the function ϕ_1' (here written in a discrete form) being estimated from the knowledge of the bundle orientation (here captured from the microtomography images). Compared to the hydrodynamic forces proposed by Servais *et al.* (1999a), the proposed Eqs. (16)–(18) account for (i) the dependence of contact surfaces on the bundle orientation and (ii) the influence of the confining pressure p. It requires only two constitutive parameters to be estimated, i.e., the equivalent sheared thickness $\bar{e}$ and the pressure p_0. These parameters were determined from the experimental data plotted in Fig. 10 and set to 1.5×10^{-5} m and $45\,000$ Pa, respectively.

3. Comparison with the pull-out experiments

As shown in Fig. 10, the simple pull-out model described by Eqs. (14)–(18) gives a rather good fit of the experimental data. Even if this should be confirmed and

strengthened by other experimental data, all the experimental trends seem to be correctly captured by the model: effects of the pull-out velocity, confining stress, fiber content, interaction between the suspending fluid and the continuous bundle [see the dotted line in graph of Fig. 10(c)].

D. Coming back to σ^{ff}

It is now possible to write more precisely the expression of the stress contribution σ^{ff} given in Eq. (2) and involved in the definition of the suspension stress σ^s [Eq. (1)].

- The results obtained in Subsection VI A tend to validate the use of elementary soft core approaches to model the microstructures of the considered fiber bundle suspensions. Thus, the number of bundle–bundle contacts N_c^{rev} contained inside a representative elementary volume V^{rev} of the suspension, together with the vectors $\mathbf{G_iG_j}$ involved in Eq. (2), can be estimated from numerical procedures involving these types of soft core assumptions [Dumont *et al.* (2009); Le Corre *et al.* (2005); Vassal *et al.* (2008)], or using directly the analytical tube model and assuming the spatial homogeneity of the suspension at the microscale [Alkhagen and Toll (2007); Djalili-Moghaddam and Toll (2005); Férec *et al.* (2009a) Servais *et al.* (1999a); Toll and Månson (1994); Vassal *et al.* (2008)].
- Thanks to the previous observations, a suitable expression of the tangential components $\mathbf{f}_t^k$ of $\mathbf{f}^k$ can be proposed. Indeed, these forces can be directly deduced from the averaged contact force $\bar{f}^f$ defined in Eq. (17), by replacing the averaged contact surface $\bar{S}$ and the pull-out velocity v_e by proper expressions, i.e., by the considered contact surface S^k Eq. (5) and the relative tangential velocity $\Delta\mathbf{v}_t^k = \mathbf{v}_t^i - \mathbf{v}_t^j$ between contacting bundles i and j, respectively:

$$\mathbf{f}_t^k = \mu_0 \frac{d_{max}^2}{||\overline{\mathbf{p}}^i \times \overline{\mathbf{p}}^j||}\left(1 + \frac{p}{p_0}\right)\left(1 + \left(\frac{1}{\dot{\gamma}_c}\frac{||\Delta\mathbf{v}_t^k||}{e}\right)^2\right)^{\frac{n-1}{2}}\frac{\Delta\mathbf{v}_t^k}{e}. \tag{19}$$

In this equation, the relative orientation between contacting bundles i and j and needed to calculate $||\overline{\mathbf{p}}^i \times \overline{\mathbf{p}}^j||$ can be estimated numerically or by the use of the tube model (see the first previous point). Similarly, approximations of the relative tangential velocity $\Delta\mathbf{v}^k$ can be established from particle level simulations [Ausias *et al.* (2006); Dumont *et al.* (2009); Fan *et al.* (1998); Joung *et al.* (2001); Le Corre *et al.* (2005); Sundararajakumar and Koch (1997); Switzer and Klingenberg (2003)] or by using analytical assumptions concerning the kinematics of fiber bundles [Alkhagen and Toll (2007); Djalili-Moghaddam and Toll (2005); Férec *et al.* (2009a); Servais *et al.* (1999a); Toll and Månson (1994)].

- To fully specify the stress contribution σ^{ff}, the normal components $f_n^k\overline{\mathbf{q}}^k$ of $\mathbf{f}^k$ have to be established too. These forces are directly connected to the deformation of the fibrous network occurring either during the suspension processing (mainly occurring by packing mechanisms that induce the consolidation of the fibrous networks) or during the suspension flow (mainly occurring by elongational and shear flows under confined stress states at more of less constant fiber content). Various micromechanisms can induce these forces: bending, torsion, longitudinal, and transverse tension/compression of bundles. Some theories have been established to estimate them analytically under simplifying assumptions [Alkhagen and Toll (2007); Toll (1998); Toll and Månson (1994); van Wyk (1946)]. The validity of these theories in the case of fibrous networks made up of fiber bundles is not straightforward [Servais *et al.* (1999a)]. Some work is still needed to better

estimate such mechanisms analytically. But it remains possible to estimate the effect of $f_n^k \overline{\mathbf{q}}^k$ on the overall suspension stress $\boldsymbol{\sigma}^s$ by analyzing the consolidation and the lubricated compression experiments performed in Sec. IV. Indeed, during the consolidation experiments, the pressure term $-p\boldsymbol{\delta}$ and the contributions $\boldsymbol{\sigma}^m$ and $\boldsymbol{\sigma}^{fm}$ are negligible so that $\boldsymbol{\sigma}^s \approx \boldsymbol{\sigma}^{ff}$. By assuming for simplicity a planar bundle orientation normal to the packing direction $\mathbf{e}_3$, by noting $\mathbf{G_i G_j} = x_l^k \mathbf{e}_l$, the macroscopic packing stress $\boldsymbol{\sigma}_{33}^s$ reads

$$\boldsymbol{\sigma}_{33}^s \approx \boldsymbol{\sigma}_{33}^{ff} = n_c \frac{1}{N^{rev}} \sum_{N^{rev}} x_3^k f_n^k. \tag{20}$$

As shown in Fig. 7, for $\phi = 0.13$, the stress σ_{33}^{ff} never exceeds 200 Pa and gives an estimate of the order of magnitude of the contribution of contact forces $f_n^k \overline{\mathbf{q}}^k$ to the overall behavior of the studied suspension. This low value is related, in particular, to the weak bending rigidity of fiber bundles when they are bent along their smallest thickness d_{min}.

At the same time, during the lubricated compression of the suspension, i.e., when the flow of the suspension exhibits a homogeneous and nearly incompressible one-phase flow, the suspension stress σ_{33}^s is expressed as

$$\sigma_{33}^s = n_c \frac{1}{N^{rev}} \sum_{N^{rev}} x_3^k f_n^k - n_c \frac{1}{N^{rev}} \sum_{N^{rev}} x_1^k f_{t1}^k + \sigma_{33}^m - \sigma_{11}^m + \sigma_{33}^{fm} - \sigma_{11}^{fm}. \tag{21}$$

As for the consolidation tests, the first term of the last equation is induced by the bending of bundles, and its magnitude can be considered to be close to that recorded during the consolidation tests when $\phi = 0.13$, i.e., ≈ 200 Pa. Please note that it is also possible to get an estimation of the second term of Eq. (21), (i) from the 3D micrograph analyzed in Sec. III (Fig. 4), (ii) by assuming that the motion of fiber bundles is an affine function of the velocity gradient, and (iii) from the contact law (19) stated previously. Indeed, point (i) provides the bundles' position, orientation, connectivity, and contact surfaces. Together with point (i), point (ii) allows the relative velocities between bundles at their contact points to be roughly estimated. Both points are finally useful to achieve point (iii). Doing so, it is found that the second stress contribution is ranging within approximately 2000 and 4000 Pa (depending on the confining pressure estimated from Fig. 6). Of course, this result should be taken cautiously and should be confirmed using other similar 3D micrographs. Nonetheless, the three following comments can be made about this result:

• It shows that the second term of Eq. (21) (i) is much higher than the first and (ii) contributes significantly to the overall macroscopic stress levels recorded in Fig. 6. Hence, during the typical incompressible flow situations encountered when molding by compression the considered composites, the effect of the normal component of contact forces $f_n^k \overline{\mathbf{q}}^k$ on the overall behavior of the suspension may be negligible compared with the role played by the tangential components $\mathbf{f}_t^k$ of $\mathbf{f}^k$, at least for the tested experimental conditions. This point is in agreement with the assumptions stated in the multiscale model established by Le Corre *et al.* (2005) for SMC. This result may also explain why dry Coulombic forces were negligible compared with viscous forces in the case of the pull-out experiments.

• This result also shows that the stress contribution $\boldsymbol{\sigma}^{ff}$ induced by bundle–bundle contacts cannot be neglected during the lubricated compression experiments displayed in Fig. 6, where the moderate bundle content ($\phi = 0.13$) induces a restricted number of bundle–bundle contacts per unit of volume n_c. It is clear that for higher fiber contents

and/or slenderer fiber bundles, the role of $\boldsymbol{\sigma}^{ff}$ may increase rapidly. Indeed, according to the tube model Eq. (11) and to the definition of $n_c \approx 2\bar{Z}\phi/(\pi d_{max}d_{min}l)$, the stress contribution $\boldsymbol{\sigma}^{ff}$ defined in Eq. (2) is expected to be a quadratic and a linear function of ϕ and l/d_{max}, respectively.

- At the same time, it is important to notice that this result also proves that the other stress contributions, i.e., $\boldsymbol{\sigma}^{fm}$ and $\boldsymbol{\sigma}^{m}$, should not be neglected to estimate the overall suspension stress. Unfortunately, it was not possible to estimate them using analytical models proposed in the literature (see the corresponding references given in the Introduction). Indeed, these models were developed considering assumptions that are not fulfilled in the studied suspensions. These latter are neither dilute nor semidilute. The suspending fluid is neither Newtonian nor a power-law fluid.

VII. CONCLUSION

The first aim of this study was to analyze the fibrous microstructures of concentrated planar fiber suspensions very close to the polymer composites reinforced with fiber bundles such as SMC, GMT, or CMT. For that purpose, an original analysis of 3D micrographs obtained from x-ray microtomography at various spatial resolutions was carried out. Despite the difficulties encountered to use automatic image analysis subroutines, the obtained results emphasize that x-ray microtomography is a powerful tool to analyze the microstructures of such materials and to discuss some of the microstructure assumptions stated in the multiscale models of the literature:

- The fine description of the bundle architecture proved that fiber bundles were rather straight, mainly orientated in the principal plane of the studied planar suspensions.
- It was also possible to detect bundle–bundle contacts, to analyze the geometry of contact surfaces, mainly looking like planar rhombs, and to estimate the coordination number of the considered suspensions, i.e., the number of bundle–bundle contacts per bundle. It seems that the statistical soft core tube model appears as a simple but accurate enough microstructure model for the studied fiber bundle suspensions. Analyzing the fibrous architecture and the fiber coordination number of other scanned volumes would be a way to strengthen this.
- X-ray microtomography was also successfully used to validate the test conditions of the pull-out experiments (see Appendix B), i.e., by showing that the continuous extracted bundle was straight and that its motion did not greatly affect its surrounding fibrous architecture. This is another interesting use of such a technique. Work in progress is now focusing on *in situ* observations during pull-out experiments, e.g., in order to detect possible geometrical changes in contact zones, or on standard microrheometry experiments, as already done for suspensions of aligned fibers [Latil *et al.* (2011)].
- From the two last points, it was finally possible (i) to analyze the pull-out experiments and (ii) to estimate the fiber stress contribution, both without any *a priori* assumptions concerning the fibrous microstructures.

The second objective of this study was to analyze the deformation micromechanisms of the considered suspensions. For this reason, pull-out experiments were carried out by using a specially designed apparatus, the validity of which was checked for the suspending fluid and for the suspensions (by using the microtomography, see above):

- Whatever the investigated test conditions, the recorded extraction forces exhibit no noticeable yield force and reflect a fluidlike behavior. Such a phenomenological micromechanical behavior is also in agreement with observations made at the macroscale during lubricated compression tests. It suggests that flow mechanisms in bundle–

bundle contacts are mainly ruled by lubrication forces induced by the shearing of the suspending fluid entrapped in contact zones.

- The influences of the pull-out velocity v_e, confining stress σ_n, and bundle content ϕ on the pull-out force f_e were also investigated. f_e evolves as a power-law of v_e, with a power-law exponent identical to that measured by the suspending fluid at high shear rates. f_e is an affine function of the confining stress. Such a trend that cannot be neglected is related to pressure-induced modifications of contact zones. To be confirmed, this point would deserve *in situ* observations of contact zones (see above). Lastly, f_e is an affine function of ϕ, the influence of ϕ on f_e being significant and directly connected to the coordination number along the extracted fiber bundle.

- It was also shown that the extraction force induced by hydrodynamic interactions between the suspending fluid and the extracted bundle away from contact zones was of the same order of magnitude than that induced by bundle–bundle contacts. A phenomenological expression was proposed to describe it, built on results of simplified numerical calculations of the fluid flow problem in zones far from contacts.

- The two last points were used to propose a pull-out model. From the knowledge of the fibrous microstructure and the rheology of the suspending fluid, this model requires few additional constitutive parameters and gives a correct fit of the acquired experimental data.

- From this model, it was possible to propose a micromechanical model to predict the contribution of bundle–bundle contacts to the overall behavior of concentrated fibrous suspensions.

- In parallel, these microscale results were used to discuss some of the assumptions stated in multiscale models dedicated to concentrated fiber suspensions. In future studies, they could also be used to improve their micromechanics. For example, to date, no rheological model for concentrated fiber suspensions takes into account the role of the confining fluid pressure on the fiber stress tensor contribution $\boldsymbol{\sigma}^{ff}$. In addition, no model proposes a suitable form for the stress contributions $\boldsymbol{\sigma}^m$ and $\boldsymbol{\sigma}^{fm}$ that would be relevant in the concentrated regime and for non-Newtonian fluid.

APPENDIX A: VALIDITY OF THE PULL-OUT TEST FOR THE SUSPENDING FLUID

- To see whether the trend shown in Fig. 10(b) is purely due to the rheology of the suspending fluid [that behaves as a Carreau fluid, see Fig. 1(a)] and not induced by any artifact of the pull-out device, the pull-out test was numerically simulated and an inverse method was carried out to determine the constitutive parameters of the Carreau–Yasuda model (3) giving the best fit of the data of Fig. 10(b). For that purpose, the direct 2D fluid flow problem was solved inside the suspending fluid flow domain Ω_m by using the finite element code COMSOL [Orgéas *et al*. (2007)] to solve a mixed velocity-pressure formulation of the problem and P2-P1 finite elements [see a zoom of the mesh around the cross section of the bundle in Fig. 12(b)]

$$\begin{cases} \nabla \cdot (2\mu(\dot{\gamma})\mathbf{D}) = \nabla p & \text{in} \quad \Omega_m \\ \mathbf{v} = v_e \mathbf{e_1} & \text{on} \quad \Gamma_e \\ \mathbf{v} = \mathbf{0} & \text{on} \quad \Gamma \end{cases} \quad (A1)$$

In the above boundary value problem, up to an arbitrary pressure, the unknowns are the 3D velocity field $\mathbf{v}$ and the pressure field p, both being functions of only the two space variables x_2 and x_3. Furthermore, $\mathbf{D}$ and $\dot{\gamma}$ are the strain rate tensor and the generalized shear rate, respectively. Besides, the viscosity $\mu(\dot{\gamma})$ follows the Carreau–Yasuda law (3). Lastly, to run the simulation, the extraction velocity v_e was prescribed on the external surface Γ_e of the extracted bundle, whereas the velocity was set to zero on the lateral surfaces Γ of the pull-out device. The optimization of the inverse method was carried out by using MATLAB and by following the Nelder–Mead algorithm used for multidimensional unconstrained nonlinear minimization. μ_0, a, and $\dot{\gamma}_c$ were the three constitutive parameters to be determined: by using theoretical results of homogenization [Auriault *et al.* (2002); Idris *et al.* (2004); Orgéas *et al.* (2006, 2007)], n was directly set to the value found in rheometry experiments. As shown from the continuous line plotted in Fig. 12(a), the results of the inverse method show a very good fit of the experimental results. Furthermore, this fit is reached for constitutive parameters very close to those measured by the cone-plate rheometer (Sec. II A), i.e., $\mu_0 = 27\,030$ Pa s, $a = 2.02$, and $\dot{\gamma}_c = 2.03 \times 10^{-2}\,\text{s}^{-1}$, thus validating the pull-out tests for the suspending fluid.

APPENDIX B: VALIDITY OF THE PULL-OUT TEST FOR THE SUSPENSIONS

To analyze properly deformation micromechanisms from the curves shown in Figs. 8(b) and 9, it was important to check whether the extraction of the continuous bundles did not disturb significantly their surrounding fibrous microstructure during the pull-out experiments. Up to now, this is an *a priori* assumption which has never been validated [Caba *et al.* (2007); Servais *et al.* (1999a, 1999b)]. By combining pull-out tests and x-ray microtomography, it was possible to answer questions concerning this crucial point. To do so, three scans were carried out using a sample subjected to an interrupted pull-out test, utilizing testing conditions similar to those given in Fig. 8(b). The first scan was achieved in the initial state. It corresponds to the micrograph (c) in Fig. 2. The second scan was done at the peak force observed in Fig. 8(b) and the last scan at the end of the experiments, i.e., at $L_e = 20$ mm. By using these scans, it was possible, as shown in Fig. 2(c), (i) to measure the angles α_i between the continuous bundle and its contacting visible short bundles i, together with the distance d_{ij} between adjacent visible short bundles i and j in contact with the extracted bundle, and (ii) to estimate the mean length and the angle ratios $\langle d_{ij}/d_{ij}^0 \rangle$ and $\langle \alpha_i/\alpha_i^0 \rangle$, d_{ij}^0 and α_i^0 being measured in the initial state. At the peak force, these ratios, respectively, equal to 0.9 and 1, whereas they equal 0.87 and 1.07 at the end of the test. These ratios prove that very weak variations of the tested microstructures were induced during the very large displacement the continuous bundle was subjected to during a pull-out test.

References

Advani, S. G., *Flow and Rheology in Polymer Composites Manufacturing, Composite Materials Series* (Elsevier, Amsterdam, The Netherlands, 1994), Vol. 10.

Advani, S. G., and C. L. Tucker, "The use of tensors to describe and predict fiber orientation in short fiber composites," J. Rheol. **3**(8), 751–784 (1987).

Alkhagen, M., and S. Toll, "Micromechanics of a compressed fiber mass," J. Appl. Mech. **74**, 723–731 (2007).

Auriault, J.-L., P. Royer, and C. Geindreau, "Anisotropic filtration law for power-law fluids," Int. J. Eng. Sci. **40**(10), 1151–1163 (2002).

Ausias, G., X. Fan, and R. Tanner, "Direct simulation for concentrated fibre suspensions in transient and steady state shear flows," J. Non-Newtonian Fluid Mech. **135**, 46–57 (2006).

Badel, P., E. Vidal-Salle, E. Maire, and P. Boisse, "Simulation and tomography analysis of textile composite reinforcement deformation at the mesoscopic scale," Compos. Sci. Technol. **68**, 2433–2440 (2008).

Balberg, I., C. Anderson, S. Alexander, and N. Wagner, "Excluded volume and its relation to the onset of percolation," Phys. Rev. B **30**(7), 3933–3943 (1984).

Baruchel, J., J. Y. Buffière, P. Cloetens, M. Di Michiel, E. Ferrie, W. Ludwig, E. Maire, and L. Salvo, "Advances in synchrotron radiation microtomography," Scr. Mater. **55**, 41–46 (2006).

Batchelor, G. K., "Slender-body theory for particles of arbitrary cross-section in Stokes flow," J. Fluid Mech. **44**(3), 419–440 (1970).

Batchelor, G. K., "The stress generated in a non-dilute suspension of elongated particles by pure straining motion," J. Fluid Mech. **46**(4), 813–829 (1971).

Berglund, L. A., and M. L. Ericson, "Glass mat reinforced polypropylene," in *Polypropylene: Structure, Blends and Composites*, edited by J. Karger-Kocis (Chapman and Hall, London, 1995), Chap. 5.

Caba, A., A. Loos, and R. Batra, "Fiber-fiber interaction in carbon mat thermoplastics," Composites, Part A **38**, 469–483 (2007).

Chalencon, F., L. Orgéas, P. Dumont, G. Foray, J. Cavaillé, E. Maire, and S. Rolland du Roscoat, "Lubricated compression and x-ray microtomography to analyse the rheology of a fibre-reinforced mortar," Rheol. Acta **49**, 765–777 (2010).

Dinh, M. S., and R. C. Armstrong, "A rheological equation of state for semiconcentrated fiber suspensions," J. Rheol. **28**(3), 207–227 (1984).

Djalili-Moghaddam, M., and S. Toll, "A model for short-range interactions in fibre suspensions," J. Non-Newtonian Fluid Mech. **132**, 73–83 (2005).

Doi, M., and S. F. Edwards, "Dynamics of rod-like macromolecules in concentrated solution," J. Chem. Soc., Faraday Trans. 2 **74**(1), 560–570 (1978).

Ducloux, R., M. Vincent, J.-F. Agassant, and A. Poitou, "Simulation of compression molding of long-glass-fiber-reinforced thermoplastic sheets," Polym. Compos. **13**(1), 30–37 (1992).

Dumont, P. J. J., S. Le Corre, L. Orgéas, and D. Favier, "A numerical analysis of the evolution of bundle orientation in concentrated fibre-bundle suspensions," J. Non-Newtonian Fluid Mech. **160**, 76–92 (2009).

Dumont, P., J.-P. Vassal, L. Orgéas, V. Michaud, D. Favier, and J.-E. Månson, "Processing, characterization and rheology of transparent concentrated fibre bundle suspensions," Rheol. Acta **46**, 639–651 (2007).

Dumont, P., L. Orgéas, S. Le Corre, and D. Favier, "Anisotropic viscous behavior of sheet molding compounds (SMC) during compression molding," Int. J. Plast. **19**(4), 625–646 (2003).

Ericsson, K. A., S. Toll, and J.-A. E. Månson, "Sliding plate rheometry of planar oriented concentrated fiber suspension," Rheol. Acta **36**, 397–405 (1997).

Fan, X., N. Phan-Thien, and R. Zheng, "A direct simulation of fibre suspensions," J. Non-Newtonian Fluid Mech. **74**, 113–135 (1998).

Férec, J., G. Ausias, M. C. Heuzey, and P. J. Carreau, "Modeling fiber interactions in semiconcentrated fiber suspension," J. Rheol. **53**, 49–72 (2009a).

Férec, J., M. C. Heuzey, J. Pérez-González, L. de Vargas, G. Ausias, and P. J. Carreau, "Investigation of the rheological properties of short glass fiber-filled polypropylene in extensional flow," Rheol. Acta **48**, 59–72 (2009b).

Folgar, F., and C. L. Tucker, "Orientation behavior of fibers in concentrated suspensions," J. Reinf. Plast. Compos. **3**, 98–118 (1984).

Gibson, A., and S. Toll, "Mechanics of the squeeze flow of planar fibre suspensions," J. Non-Newtonian Fluid Mech. **82**, 1–24 (1999).

Goddard, J. D., "Tensile stress contribution of flow-oriented slender particles in non-Newtonian fluids," J. Non-Newtonian Fluid Mech. **1**, 1–17 (1976).

Idris, Z., L. Orgéas, C. Geindreau, J. F. Bloch, and J. L. Auriault, "Microstructural effects on the flow of power-law fluid through fibrous media," Modell. Simul. Mater. Sci. Eng. **12**, 995–1016 (2004).

Joung, C. G., N. Phan-Thien, and X. J. Fan, "Direct simulation of flexible fibers," J. Non-Newtonian Fluid Mech. **99**, 1–36 (2001).

Joung, C. G., N. Phan-Thien, and X. J. Fan, "Viscosity of curved fibers in suspension," J. Non-Newtonian Fluid Mech. **102**, 1–17 (2002).

Komori, T., and K. Makishima, "Numbers of fiber-to-fiber contacts in general fiber assemblies," Text. Res. J. **47**, 13–17 (1977).

Komori, T., and M. Itoh, "A modified theory of the fiber contact in general fiber assemblies," Text. Res. J. **64**, 519–528 (1994).

Latil, P., L. Orgéas, C. Geindreau, P. J. J. Dumont, and S. Rolland du Roscoat, "Towards the 3D in situ characterisation of deformation micro-mechanisms within a compressed bundle of fibres," Compos. Sci. Technol. **71**, 480–488 (2011).

Le, T., P. Dumont, L. Orgéas, D. Favier, L. Salvo, and E. Boller, "X-ray phase contrast microtomography for the analysis of the fibrous microstructure of SMC composites," Composites, Part A **39**, 91–103 (2008).

Le Corre, S., D. Caillerie, L. Orgéas, and D. Favier, "Behavior of a net of fibers linked by viscous interactions: Theory and mechanical properties," J. Mech. Phys. Solids **52**, 395–421 (2004).

Le Corre, S., L. Orgéas, D. Favier, A. Tourabi, A. Maazouz, and C. Venet, "Shear and compression behavior of sheet molding compounds," Compos. Sci. Technol. **62**(4), 571–577 (2002).

Le Corre, S., P. Dumont, L. Orgéas, and D. Favier, "Rheology of highly concentrated planar fiber suspensions," J. Rheol. **49**, 1029–1058 (2005).

Lipscomb, G. G., M. M. Denn, D. U. Hur, and D. V. Boger, "The flow of fiber suspensions in complex geometries," J. Non-Newtonian Fluid Mech. **26**, 297–325 (1988).

Mackaplow, M. B., and E. S. G. Shaqfeh, "A numerical study of the rheological properties of suspensions of rigid, non-Brownian fibres," J. Fluid Mech. **329**, 155–186 (1996).

Odenberger, P., H. Andersson, and T. Lundström, "Experimental flow-front visualisation in compression moulding of SMC," Composites, Part A **35**, 1125–1134 (2004).

Orgéas, L., C. Geindreau, J.-L. Auriault, and J.-F. Bloch, "Upscaling the flow of generalised Newtonian fluids through anisotropic porous media," J. Non-Newtonian Fluid Mech. **145**, 15–29 (2007).

Orgéas, L., P. J. J. Dumont, J. P. Vassal, O. Guiraud, V. Michaud, and D. Favier, "In-plane conduction of polymer composites plates reinforced with architectured networks of Copper fibres," J. Mater. Sci. **45**, 2932–2942 (2012).

Orgéas, L., P. J. J. Dumont, T. H. Le, and D. Favier, "Lubricated compression of BMC, a concentrated and fibre reinforced granular polymer suspension," Rheol Acta **47**, 677–688 (2008).

Orgéas, L., Z. Idris, C. Geindreau, J.-F. Bloch, and J.-L. Auriault, "Modelling the flow of power-law fluids through anisotropic porous media at low pore Reynolds number," Chem. Eng. Sci. **61**, 4490–4502 (2006).

Osswald, T., and S.-C. Tseng, *Flow and Rheology in Polymer Composites Manufacturing, Composites Materials Series* (Elsevier, Amsterdam, The Netherlands, 1994), Vol. 10, pp. 361–413.

Pan, N., "A modified analysis of the microstructural characteristics of general fiber assemblies," Text. Res. J. **63**, 336–345 (1993).

Petrich, M. P., and D. L. Koch, "Interactions between contacting fibers," Phys. Fluids **10**(8), 2111–2113 (1998).

Petrich, M. P., D. L. Koch, and C. Cohen, "An experimental determination of the stress-microstructure relationship in semi-concentrated fiber suspensions," J. Non-Newtonian Fluid Mech. **95**, 101–133 (2000).

Ranganathan, S., and S. G. Advani, "Fiber-fiber interactions in homogeneous flows of non-dilute suspensions," J. Rheol. **35**, 1499–1522 (1991).

Rolland du Roscoat, S., M. Decain, X. Thibault, C. Geindreau, and J.-F. Bloch, "Estimation of microstructural properties from synchrotron x-ray microtomography and determination of the REV in paper materials," Acta Mater. **55**, 2841–2850 (2007).

Sandstrom, C., and C. Tucker, "A theory for concentrated fiber suspensions with strong fiber-fiber interaction," Makromol. Chem., Macromol. Symp. **68**, 291–300 (1993).

Servais, C., A. Luciani, and J. A. E. Månson, "Fiber-fiber interaction in concentrated suspensions: Dispersed fiber bundles," J. Rheol. **43**(4), 1005–1018 (1999a).

Servais, C., J. Manson, and S. Toll, "Fiber-fiber interaction in concentrated suspensions: Disperse fibers," J. Rheol. **43**(4), 991–1004 (1999b).

Shaqfeh, E. S. G., and G. Fredrickson, "The hydrodynamic stress in a suspension of rods," Phys. Fluids **2**(1), 7–24 (1990).

Silva-Nieto, R., and B. Fisher, "Rheological characterization of unsaturated polyester resin sheet molding compound," Polym. Eng. Sci. **21**(8), 499–506 (1981).

Souloumiac, B., and M. Vincent, "Steady shear viscosity of short fibre suspensions in thermoplastics," Rheol. Acta **37**, 289–298 (1998).

Sundararajakumar, R. R., and D. L. Koch, "Structure and properties of sheared fiber suspensions with mechanical contacts," J. Non-Newtonian Fluid Mech. **73**, 205–239 (1997).

Switzer, L. H., and D. J. Klingenberg, "Rheology of sheared flexible fiber suspensions via fiber-level simulations," J. Rheol. **47**(3), 759–778 (2003).

Thomasson, J. L., and M. A. Vlug, "Influence of fibre length and concentration on the properties of glass fibre-reinforced polypropylene: 1. Tensile and flexural modulus," Composites, Part A **27A**, 477–484 (1996).

Toll, S., "Note: On the tube model for fiber suspensions," J. Rheol. **37**(1), 123–125 (1993).

Toll, S., "Packing mechanics of fiber reinforcements," Polym. Eng. Sci. **38**, 1337–1350 (1998).

Toll, S., and J.-A. E. Månson, "Dynamics of a planar concentrated suspension with non-hydrodynamic interaction," J. Rheol. **38**(4), 985–997 (1994).

van Wyk, C., "Note on the compressibility of wool," J. Text. Inst. **37**, 285–292 (1946).

Vassal, J.-P., L. Orgéas, D. Favier, J.-L. Auriault, and S. Le Corre, "Upscaling the diffusion equations in particulate media made of highly conductive particles. II. Application to fibrous materials," Phys. Rev. E **77**, 011303 (2008).

Yamane, Y., Y. Kaneda, and M. Doi, "The effect of interaction of rodlike particles in semi-dilute suspensions under shear flow," J. Phys. Soc. Jpn. **64**(9), 3265–3274 (1995).

Yasuda, K., N. Mori, and K. Nakamura, "A new visualization technique for short fibers in a slit flow of fiber suspensions," Int. J. Eng. Sci. **40**, 1037–1052 (2002).